Ministry of Education and Science of Ukraine
Ternopil Ivan Puluj National Technical University
(full name of higher education institution)
Faculty of Applied Information Technologies and Electrical Engineering
(faculty name)
Department of Electrical Engineering
(full name of the department)

QUALIFYING PAPER

For the degree of

bachelor
(educational degree (educational and qualification level))

topic: **Use of Photovoltaic Systems for Autonomous Power Supply of Consumers**

Submitted by: student of 4th course group IEE-42
specialty 141
Electrical Energetics, Electrical Engineering and Electromechanics
(code and name of specialty)

	(signature)	Mamphey I.K.A. (surname and initials)
Supervisor	(signature)	Filiuk Ya.O. (surname and initials)
Standards verified by	(signature)	Filiuk Ya.O. (surname and initials)
Head of Department	(signature)	Tarasenko M. G. (surname and initials)
Reviewer	(signature)	Kozak K.M. (surname and initials)

Ternopil
2023

Ministry of Education and Science of Ukraine
Ternopil Ivan Puluj National Technical University

Faculty Applied Information Technologies and Electrical Engineering
(full name of the faculty)
Deputy Electrical engineering
(full name of the department)

APPROVED BY
Head of Department
_____ Tarasenko M. G.
(signature) (surname and initials)
« » 2023

ASSIGNMENT
for QUALIFYING PAPER

for the degree of Bachelor
(name of educational degree)
specialty 141 – Electrical Power Engineering, Electrical Engineering and Electromechanics
(code and name of specialty)
student Mamphey Isaac Kofi Amoahforo
(Full Name)

1. Paper topic Use of photovoltaic systems for autonomous power supply of consumers
Paper supervisor Filiuk Yaroslav Oleksandrovych, Ph.D.
(surname, first name, patronymic, academic degree, academic title)
Approved by university order as of "17» February 2023 No 4/7-175

2. Student's paper submission deadline June 2023

3. Initial data for the paper To study voltage stabilizer and inverter circuits, which ensures the accuracy of voltage stabilization in a wide range of loads and temperatures with a low coefficient of nonlinear distortion.

4. Paper contents (list of issues to be developed)
1. Analytical section
2. Design and layout section
3. Calculation section
4. Safety of livelihood and fundamentals of labor protection
5. General Conclusions
5.List of graphic material (with exact number of required drawings, slides)
1. Title.2. Introduction;3,4 Methods of Measuring the Characteristics of Solar Cells/Modules
5. Volt-Ampere Characteristics of Solar Cells and Other Parameters Based on Them
6. Volt-Ampere Characteristics of Solar Cells and Other Parameters; 7,8. Simulation of solar battery characteristics; 9,10,11. Energy characteristics of the autonomous photoelectric installation
12. The Operating Cyclic Capacity of the Accumulator Battery; 13. Study of output voltage stability in a single-phase inverter according to the classical adjustment algorithm; 13,14. Study of output voltage stability in a single-phase inverter according to the classical adjustment algorithm; 14,15,16,17,18,19. Study of output voltage stability in a single-phase inverter: relay voltage regulator and regulator with pulse-width modulation; 20 Conclusions

6. Advisors of paper chapters

Chapter	Advisor's surname, initials and position	Signature, date	
		assignment was given by	assignment was received by
Life Safety and the basics of labor protection			
Standard control			

7. Date of receiving the assignment February 2023

CALENDAR PLAN

No s/p	Paper stages	Paper stages deadlines	Note
1	Introduction	02/26/2023	
2	Analytical section	03/31/2023	
3	Design and layout section	04/16/2023	
4	Calculation section	04/30/2023	
5	Safety of livelihood and fundamentals of labor protection	05/14/2023	
6	Conclusions	05/31/2023	
7	Issuance of an explanatory note	03.06.2023	
8	Designing the graphic part	06/14/2023	

Student _____ (signature) Mamphey I.K.A. (surname and initials)

Paper supervisor _____ (signature) Filiuk Ya.O. (surname and initials)

ABSTRACT

A Bachelor's qualification work by Mamphey Isaac Kofi Amoahforo. Ivan Puluj Ternopil National Technical University, Faculty of Applied Information Technologies and Electrical Engineering. Department of Electrical Engineering, Group IEE-42. - Ternopil: TNTU, 2023.

Pages:66; Figures:42; Tables:6; Refrences:15.

The topic of the bachelor's qualification work: "Use of photovoltaic systems for autonomous power supply of consumers."

The aim of this work was to study the characteristics of photovoltaic systems and their use for the autonomous power supply of consumers.

In the paper, a mathematical model of the "solar power installation for consumer" system was improved, taking into account the line resistance, power, load resistance, and determining its coefficient of performance η at maximum power point. A methodology for calculating solar power installations for autonomous power supply of consumers was proposed.

The research included the study of PV system configurations, which differ in terms of open-circuit voltage, short-circuit current, and the inclusion of smoothing chokes in the AC or DC circuit.

Keywords: solar cell/module, accumulator battery, inverter, consumer.

CONTENT

INTRODUCTION

The needs of the population and industry for electricity are limited by the reserves of oil and gas, which leads to the necessity of using renewable energy sources. Currently, one of the most important tasks of the power industry is to ensure reliable and uninterrupted electricity supply to all industrial and domestic consumers.

The relevance of the research topic is to promote the development of small solar photovoltaic installations (PV) that work in parallel with the grid and in an autonomous mode and can improve the electricity supply of domestic consumers more efficiently and faster than the development of a large energy system. Therefore, this research is dedicated to the study and improvement of small solar photovoltaic installations (PV) which is relevant and of great practical significance.

The purpose and objectives of this work are to study the characteristics of photovoltaic systems and use them for autonomous consumer power supply. The goal set in the work requires solving the following tasks:

- Studying various structural variants and selecting the optimal circuit for a photovoltaic installation;

- Studying the properties of solar modules/batteries for autonomous consumer power supply;

- Studying the voltage regulator and inverter circuit that ensures voltage stabilization accuracy over a wide range of loads and temperatures with a low coefficient of nonlinear distortions.

1. ANALYTICAL SECTION

1.1. The Relevance of Solar energy

Today, solar energy is becoming more relevant than ever. Global problems with energy resources and the dependence on imported hydrocarbons force us to look for new sources of energy and for the government to invest in solar power plants and the green tariff.

Over the past three years, the total capacity of solar power plants in Ukraine has grown by 80-95% annually due to favourable geographical conditions and the world's highest green tariff. The cost of creating solar power plants decreases every year due to the improvement of production technologies for photovoltaic modules (solar panels), increasing their capacity, efficiency coefficient, and most importantly - the cost per 1 watt of battery power is decreasing every year. The pace of development of solar energy can only be compared to the IT industry revolution.

If a few years ago, solar energy could not do without subsidies and government support, then now the world markets are reaching the point of efficiency. Due to the cheapening of solar panels and systems in general, solar energy has become profitable in countries such as Germany, Spain, Italy, Japan, Mexico, the United States, and many other countries. In May 2015, an 80 MW solar power plant was commissioned in Chile, which will sell electricity on the spot market.

In 2014, solar energy for the first-time surpassed wind energy in the pace of its development, and the average price of generated electricity was 0.15-0.35 USD/kWh for industrial-scale systems. Although, for example, in Denmark, wind energy is even more profitable than coal-fired power plants. The global growth of solar power capacity in 2015 was 38 GW, and this record was broken in 2015. It is worth noting that in 2014, China became the leader in the development of solar energy in the world. Thanks to reforms in the energy sector, the country was able to achieve an annual increase in capacity of 27.4 GW, which is almost four times more than Japan, which is in second place. There are three main factors that make solar energy increasingly advantageous:

- falling prices for photovoltaic modules (solar panels);
- annual increase in the efficiency of solar modules by 2-4%;
- increasing the scale and capacity of solar power plants.

The expansion of solar power plants leads to a significant reduction in investments required for 1 W of power. For instance, in 2012 the Ukrainian solar power plant (Perovo) with a capacity of 100 MW became the largest in the world but at the moment it is not even in the top ten. There are already systems with a capacity of more than 300 MW, and even 0.5 GW giants are in the project stage. Since 2008, the prices of solar panels have decreased by 70-80% due to the optimization of production processes, logistics, and increased module efficiency. Although prices have stabilized at the moment, there is still a prospect of reducing the cost of solar modules due to new developments by scientists and the increasing scale of production.

Over the past six years, the average price of ready-made solar systems for private homes has fallen by 53%. In Germany, half of the solar installations belong to private homeowners and farmers. Since 2008, modern legislation regulating and supporting the energy market generated from renewable energy sources has been developing in Ukraine. At the moment, the green tariff in Ukraine is the highest in the world, especially for solar power plants, and is 731.98 kopecks/kW·h for powerful power plants. Of course, there are significant imperfections in the permit issuance process, but all these processes are being honed and becoming simpler every day. Thanks to the green tariff, the payback period for investments made in large solar power plants (over 50 kW) can be 4-5 years, which creates a very attractive investment climate. What makes it promising is the installation of solar panels on the roofs of large shopping and entertainment centres, wholesale warehouses, and storage facilities due to the absence of the need to withdraw agricultural land from circulation.

Over 3-4 years ago the installation of solar panels on the roofs and facades of private houses (Fig. 1.1) was only reasonable in case of one trying to avoid the many expenses that come with connection to the grid but now it can become a good investment. The green tariff for individuals is 389.34 kopecks/kW·h, but there is a restriction on capacity up to 10 kW. The absence of requirements for the content of the local component further reduces the price of private power plants. Investments in a private solar power plant on the roof should pay off within 5-6 years. Moreover, the service life of solar panels is 25-30 years, and inverters - 15-20 years. Due to the absence of moving parts, equipment malfunctions occur extremely rarely.

Over the past five years, the volume of the Ukrainian solar energy market has been growing by 80-90% annually due to increasingly attractive conditions for selling electricity at a green tariff, the cheapening of silicon raw materials and solar panels in general, and the development of the legislative framework. But the main thing is the growing environmental awareness, the desire of people to live in harmony with nature and preserve it for future generations. The installation of solar panels on the roof of a private house can have the following goals:

- the creation of a completely autonomous solar system;
- the creation of a solar backup power system;
- selling electricity to the grid at a "green" tariff.

In the future, the solar energy sector is likely to grow at a pace no less than before. By 2030, the Ukrainian government plans to increase the capacity of solar power plants by 8.4 times.

Figure 1.1 - A PV installation located on the roof of a residential building.

1.2. Efficiency of Photovoltaic Cells/Modules and Factors Influencing It

The power of solar radiation at a distance of 150 million km from the Sun (in the geosphere of the Earth), without taking into account losses in the Earth's atmosphere, is

about 850-1450 W/m^2, depending on the geographic location. At the same time, the intensity (ratio of optical power to a defined area) of solar radiation in Europe can reach up to 900 W/m^2 even in very cloudy weather during the daytime. This energy can be converted into electricity using widely available crystalline solar modules with an efficiency of 14-17%. The energy potential of industrial crystalline photovoltaic modules, which are produced on a mass scale, is up to 130-140 W/m^2, at an optical power density of 1 kW/m^2. Figure 1.2 shows a comparison of the active surface areas of different types of photovoltaic converters required to produce 1000 W of electrical energy.

As seen in Figure 1.2, for most crystalline and thin-film photovoltaic converters, a significant surface area is required to obtain the same amount of energy due to their low efficiency. This limits their use in certain applications, including in network nodes, due to their geometrical dimensions. For industrial and local use, modules made of polycrystalline or monocrystalline silicon are most commonly used. Thin-film cells better receive scattered radiation and have lower power losses when individual areas are shaded during operation. They also function better at higher operating temperatures; however, due to their low efficiency, they significantly lag behind crystalline and concentrator photovoltaic units.

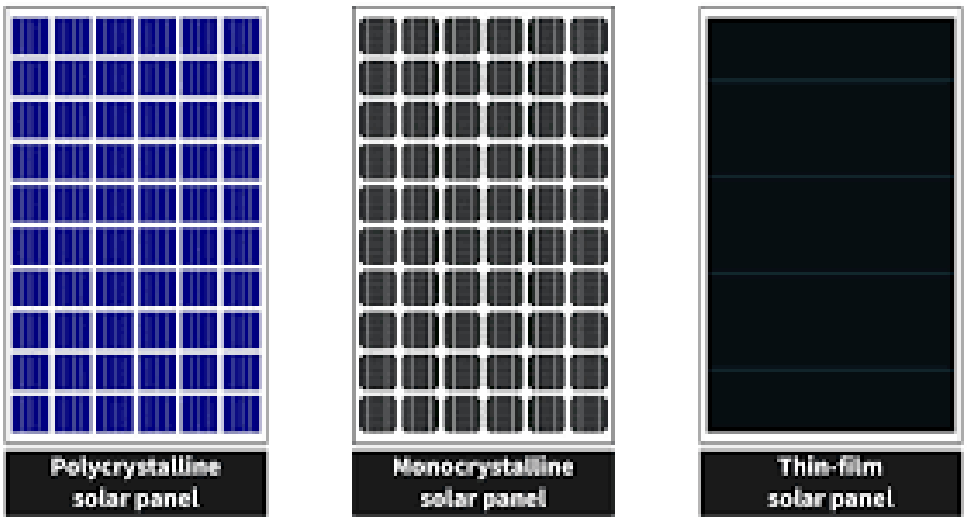

Figure 1.2- Comparison of the areas of different types of PVs for obtaining 1 kW of electric energy:for monocrystalline 6-9 m ^{2}; polycrystalline 7.5-10 m ^{2}; thin film 14-20m^2

Solar photovoltaic systems made of amorphous silicon are less commonly used due to their low efficiency and stability issues over time. Specialized thin-film technologies such as Copper Indium Diselenide and Cadmium Telluride (CdTe) are also less frequently used due to the same factors as well as the high toxicity of the chemical elements involved. However, thin-film photovoltaic converters have an advantage over crystalline ones in terms of being 10-100 times thinner and requiring less material, as well as their greater ability to convert diffuse light compared to crystalline photovoltaic converters.

Concentrator-type solar photovoltaic systems have the highest efficiency in terms of surface area. Therefore, their use is a prioritized option for creating compact systems for autonomous power supply of hardware units in information networks. In concentrator photovoltaic converters, the optical radiation energy of the solar spectrum is converted into electrical form through the internal photoelectric effect in semiconductor photovoltaic elements based on A3B5 heterostructures, silicon (Si), germanium (Ge), indium (In), arsenide (As), and gallium (Ga) materials, as well as their solid solutions SiP, GeIn, GaAsP, InGaAs, InGaAsP, and AlGaAs-GaAs. Such photovoltaic elements and modules based on them have a small effective working area, S_{eff}, of up to 1 m^2 or less, which is proportional to the percentage of the obtained energy. The output power of a photovoltaic module will be proportional to the accepted optical power intensity of the sun (I_{op}, in W/m^2), the conversion efficiency (η), the absorption coefficient (k), the effective area (S_{ef}), and the cosine of the angle of incidence (α).

$$Ppv = Ipv \times Vpv = \eta \times k \times Sef \times \cos\alpha \quad (1.1)$$

Therefore, by analysing the efficiency of photovoltaic systems, it can be concluded that disregarding cost indicators, concentrator photovoltaic modules based on GaAs are the optimal type for use in solar power plants since they have the highest efficiency with the smallest geometric dimensions. For more efficient conversion, the angle of incidence of radiation on the active surface (α) should approach 90° as closely as possible, corresponding to the condition of maximum conversion for the given values. The efficiency factor of the photovoltaic module of light energy into electrical energy is determined by the formula

$$\eta = \frac{P_{elec}}{P_{opt}} \cdot \gamma \cdot 100\% = \frac{I_p V_p}{\Phi \cdot S \cdot \sin\varphi} \cdot \gamma \cdot 100\%, \quad (1.2)$$

where I_p, V_p – operating current and voltage;

Φ – luminous flux;

S – the area of the active surface;

φ – the angle of incidence of rays;

γ – coefficient of quantum efficiency;

P_{elec}, P_{opt} – electrical and optical power.

The efficiency factor of the photocell increases with the growth of light flux Φ and photo-electromotive force U_p. However, at large values of the light flux, Φ with the increase in the concentration of free carriers, the number of their exciton recombination (fusion of electron-hole pairs) in the semiconductor structure increases. As a result of the increase in the temperature of the module, the current ΦI increase at high values, which is also the reason for the decrease in efficiency.

1.3 Spectral Characteristics of Photovoltaic Modules

The intensity of solar radiation in free space at a distance equal to the average distance between the Earth and the Sun is called the solar constant. Its value is 1353 W/m^2. When passing through the atmosphere, solar light is attenuated primarily through the absorption of infrared radiation by water vapor, ultraviolet radiation by ozone, and the scattering of radiation by atmospheric dust particles and aerosols. The atmospheric influence on the intensity of solar radiation reaching the Earth's surface is referred to as "air mass" (AM). AM is determined as the secant of the angle between the Sun and the zenith. Figure 3 shows the spectral distribution of solar radiation intensity under different conditions. The upper curve (AM0) corresponds to the solar spectrum outside the Earth's atmosphere (e.g., on board a spacecraft), i.e., at zero air mass. It is approximated by the intensity distribution of black body radiation at a temperature of 5800K. Curves AM1 and AM2 illustrate the spectral distribution of solar radiation at the Earth's surface when the Sun is at the zenith and at an angle of 600 between the Sun and the zenith, respectively. In these cases, the total radiation power is approximately

925 and 691 W/m^2, respectively. The average intensity of radiation on Earth roughly coincides with the intensity of radiation at AM = 1.5 (Sun at an angle of 450 to the horizon). Thus, with the use of high-efficiency energy conversion methods, the Sun can meet the rapidly growing energy demands virtually indefinitely.

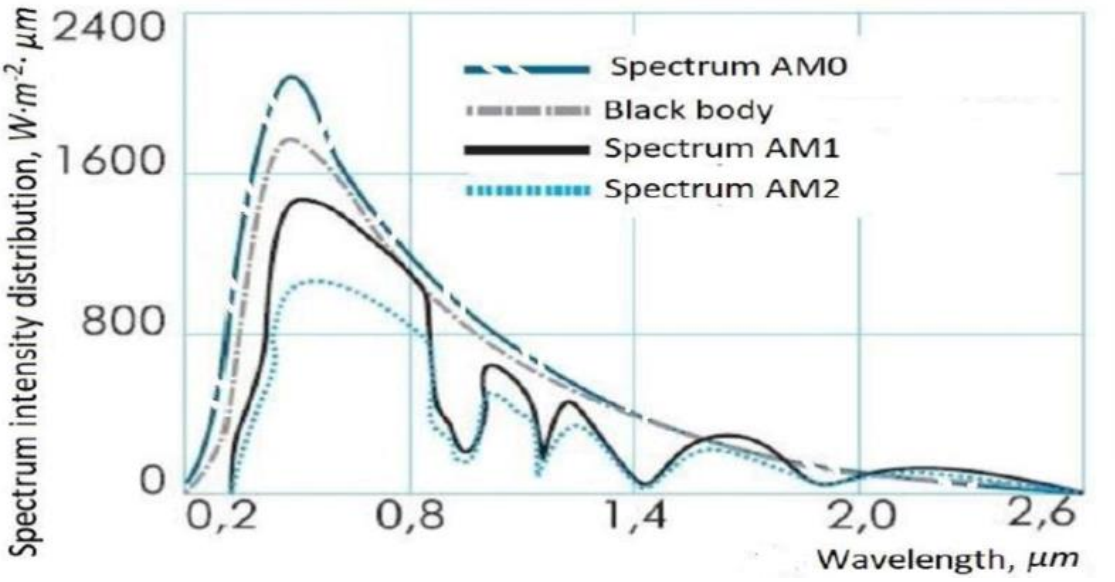

Figure1.3- Intensity distribution in the spectrum of solar radiation.

One of the main directions of direct conversion of solar energy into electricity is realized in semiconductor photovoltaic devices (PV). Until now, the production of most commercial solar cell modules has been based on crystalline Si with an efficiency of about 25% (1st generation PV) and thin-film amorphous Si with a large area PV and an efficiency of about 5-10.1% (2nd generation PV). The concept of the 3rd generation involves the use of nano- and microstructures (micro-wires). PV with micro-wires (Vapor-Liquid-Solid - VLS method) belongs to the class of devices with special structural design to achieve directed transport of charge carriers through the geometry and material of such structures. The main losses of solar radiation during its transformation into electrical energy are determined by the fundamental limitations of the photoelectric effect in the infrared radiation region (hv < Eg) and in the short-wavelength radiation region (hv >> Eg), as well as by the low efficiency of extracting photo-generated charge carriers from the volume of the crystalline silicon (C-Si) photovoltaic converter (Figure 1.4.)

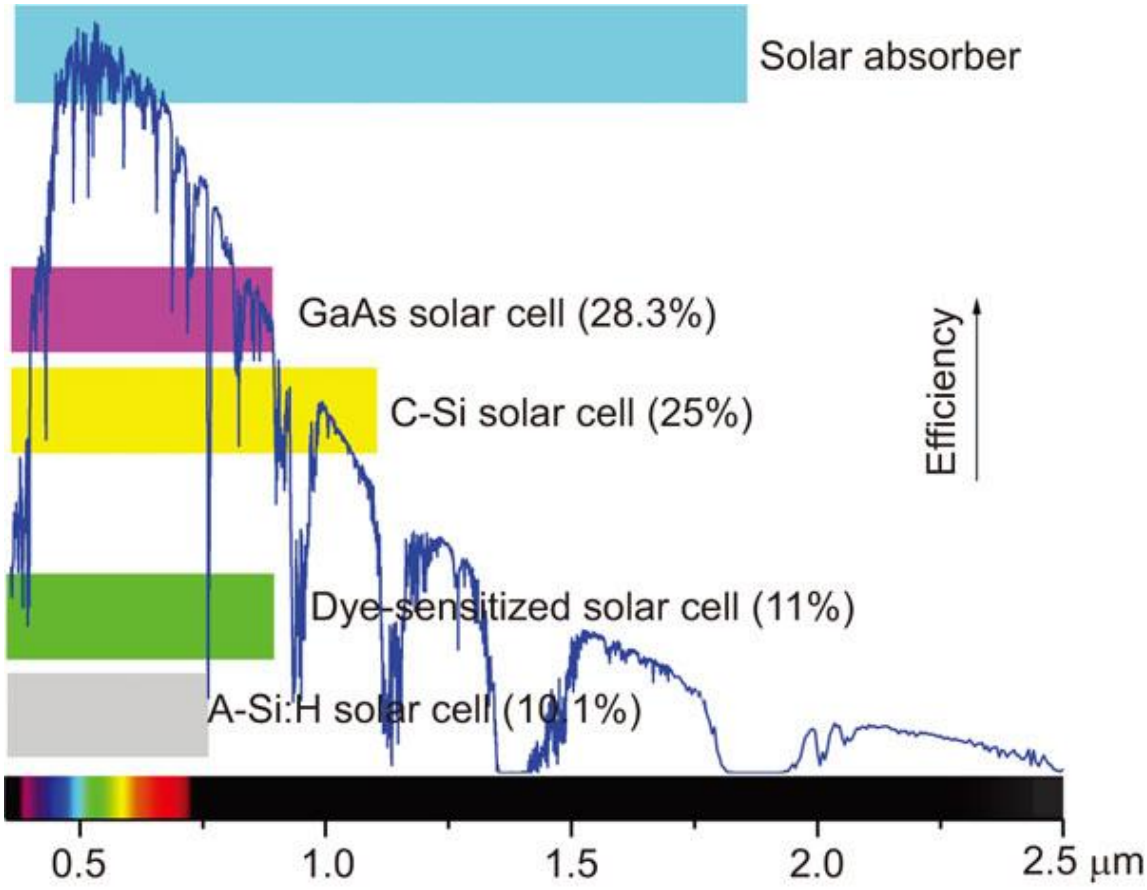

Figure1.4- Dependence of the efficiency of silicon photocells on the wavelength of solar radiation

For the production of terrestrial photovoltaic converters (PVC), the most suitable semiconductors are considered to be Si, CdTe, GaAs, and InP. Approximately 91% of the energy from incident light can be converted into electrical current in silicon-based PVC, provided that the issue of charge carrier extraction from the semiconductor volume is resolved. The low cost of silicon is a determining factor in choosing the material for photovoltaic elements.

1.4 Conclusion

Monocrystalline photovoltaic systems are the most efficient PVCs, their efficiency is 17-19%, while polycrystalline ones are 15-17%, and thin-film ones are 7-11%; however, they are also the most expensive. The radiation regime of the territory of Ukraine isfavorablee for the practical use of solar energy, so it will be profitable to use solar panels throughout Ukraine, but their use will be most effective in the southern regions.

2. DESIGN AND LAYOUT SECTION

2.1. Methods of Measuring the Characteristics of Solar Cells/Modules

To search for the optimal operating mode of a photovoltaic converter (PVC) or a solar cell (SC) under changing light flux, temperature, and electrical load parameters, it is necessary to conduct measurements and model their current-voltage characteristics (IV curves). Measuring the IV curves allows for the calculation of the maximum power and efficiency of the solar module, as well as defect monitoring at the initial stage of their usage and prediction of solar cell (SC) degradation. Based on the IV curves, load correction can also be performed for maximum power extraction.

The main methods of IV curve measurement can be divided into two classes:

- Static or continuous methods (static measurements, DC measurements).
- Dynamic or pulse methods (dynamic IV measurements, pulsed IV measurements).

Depending on the state of the SC during IV curve measurements, isothermal and isodynamic methods can be distinguished. Isothermal measurements refer to measurements where the SC temperature is maintained at a constant level, which reduces thermal distortions of the IV curves and can significantly increase the accuracy of the results. Isodynamic measurements are performed in such a way that the charge caused by carrier trapping on parasitic energy levels of the semiconductor remains unchanged during the IV curve measurement. The main goal of isodynamic measurements is to improve the accuracy of IV curve measurements by preventing or stabilizing the carrier trapping effect.

A static isothermal method was used for the IV curve measurement. For this purpose, a laboratory setup was assembled, which includes a solar radiation simulator, voltmeter V7-16, ammeter E525, and a resistor bank. Its external appearance is shown in Figure 2.1.

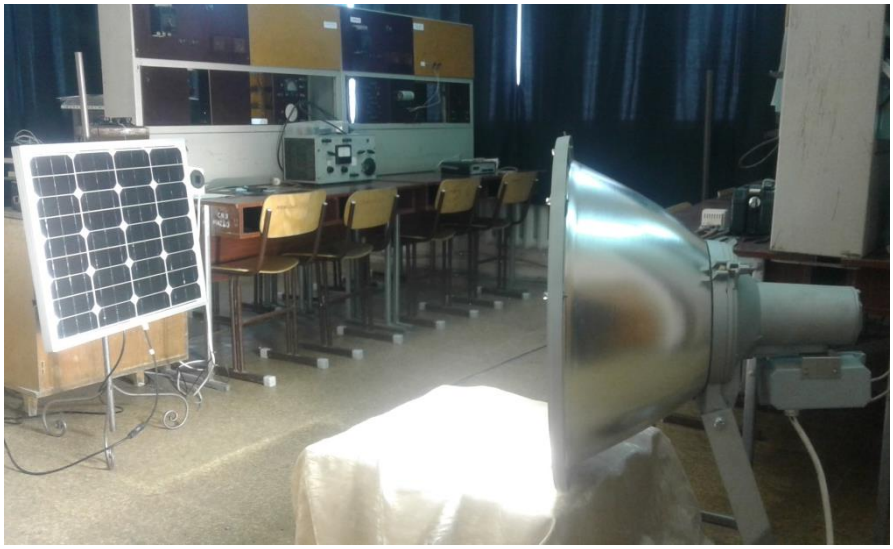

Figure 2.1- Installation for measuring the AC current of the Solar module.

DKSSH-150 and DRY-1000 gas discharge lamps were used as a simulator. The spectral composition of radiation from a lamp with xenon filling and the spectrum of solar radiation are shown in Fig. 2.2. Also figure 2.2 shows that these spectra are very close in the visible region.

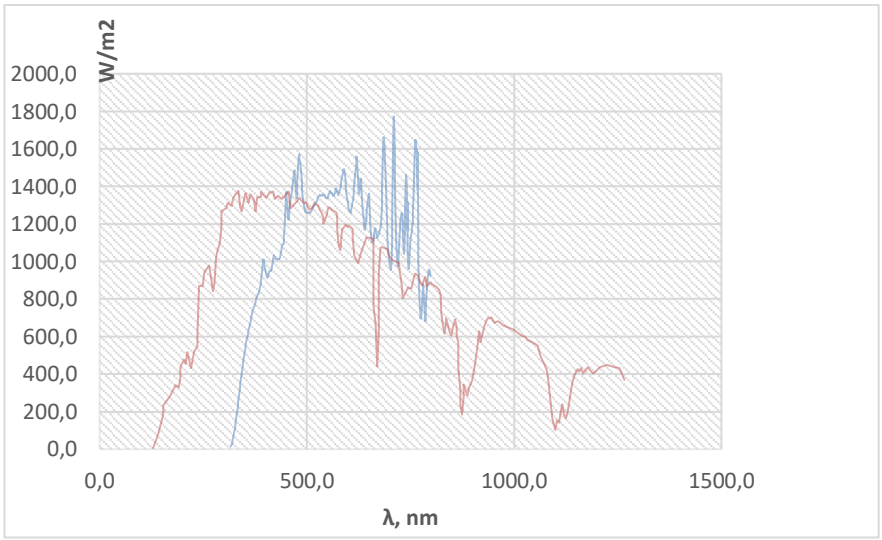

Figure 2.2- Spectral distribution of radiation from the sun and a xenon lamp.

Measurements were carried out for both light and dark current-voltage characteristics (IV curves) of the ALM-50M solar battery. The light flux incident on the solar battery was measured using the Solar Power Meter CEM DT-1307, with an error not exceeding 5%. To achieve a standardized optical radiation flux density of 1000

W/m^2, the light instrument GO-07 with a DRI-1000 lamp was used (Figure 2.1). The flux density variation was achieved by changing the distance between the light instrument and the solar battery. The change in light flux density was achieved by varying the distance between the light instrument and the solar battery. This ensured a flux density change within the range of 200 to 1000 W/m^2. The temperature of the solar battery was maintained at a constant level of 25°C. The variation of current in the load circuit and voltage across the solar battery was achieved by changing the load resistance $R_н$, using the resistor bank MSR. To study the photovoltaic parameters of the solar battery under low irradiance levels of 15-35 W/m^2, which are often observed in conditions of increased cloudiness, the light instrument FYGT300-I R7S with a DKS-150 lamp was used. The image of this setup is shown in Figure 2.3.

Figure 2.3- Installation for measuring the AC current of the SB with the DKSSH-150 lamp.

2.2. Volt-Ampere Characteristics of Solar Cells and Other Parameters Based on Them

Solar panels can be used for lighting in populated areas, just like other alternative energy sources. However, unlike them, solar panels rely on the amount of light that

reaches their surface. For example, during cloudy weather, clouds can significantly reduce the power output of a solar panel, even up to 50%. Additionally, even a small defect in the solar elements can decrease the overall efficiency, even within a batch of batteries. Therefore, to ensure the desired power output, it is necessary to sort the elements based on their parameters. Silicon solar elements cannot be described by a simple Ohm's law as they are non-linear components. Instead, volt-ampere characteristics (VAC) can be used to explain the characteristics of the element.

Figures 2.4 show the light VAC of the ALM-50M solar panel, and Figure 2.5 presents the graphs of power consumption recorded at irradiance levels of 1000, 700, 400, 200, 35, and 15 W/m^2.

On the light VAC at irradiance levels of 1000, 700, 400, and 200 W/m^2, the current SB changes very little when the voltage varies from 0 to 15 V. A sharp drop in the photocurrent occurs within the 19-22 V range. This drop allowed the determination of the value of the series resistance Rp in the equivalent circuit of the solar panel (Figures 2.4). At irradiance levels of 35 and 15 W/m^2, the same range with a small slope angle to the voltage axis is present up to 12 V. At higher voltage levels, a sharp drop in photocurrent occurs.

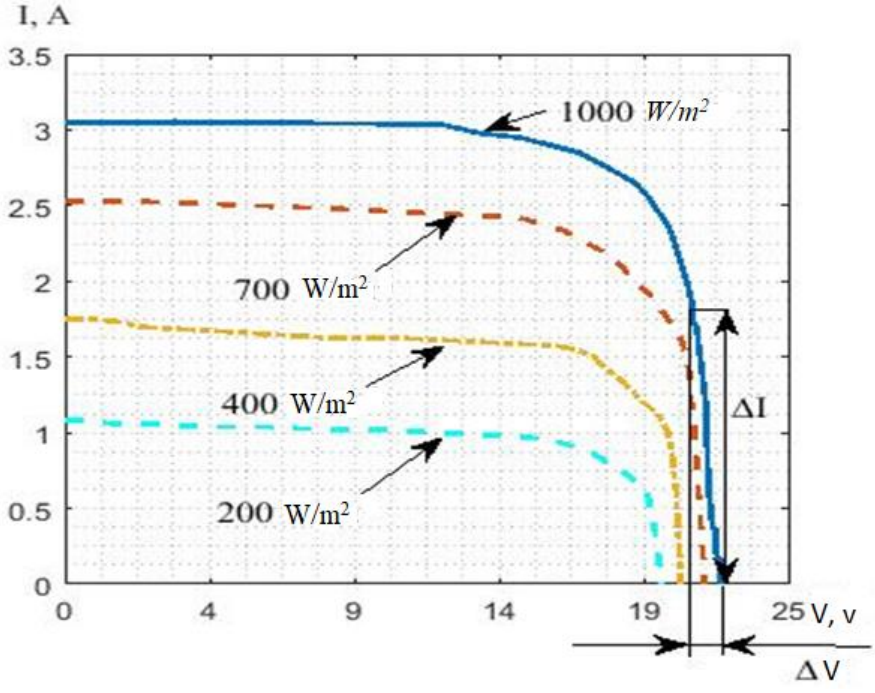

a)

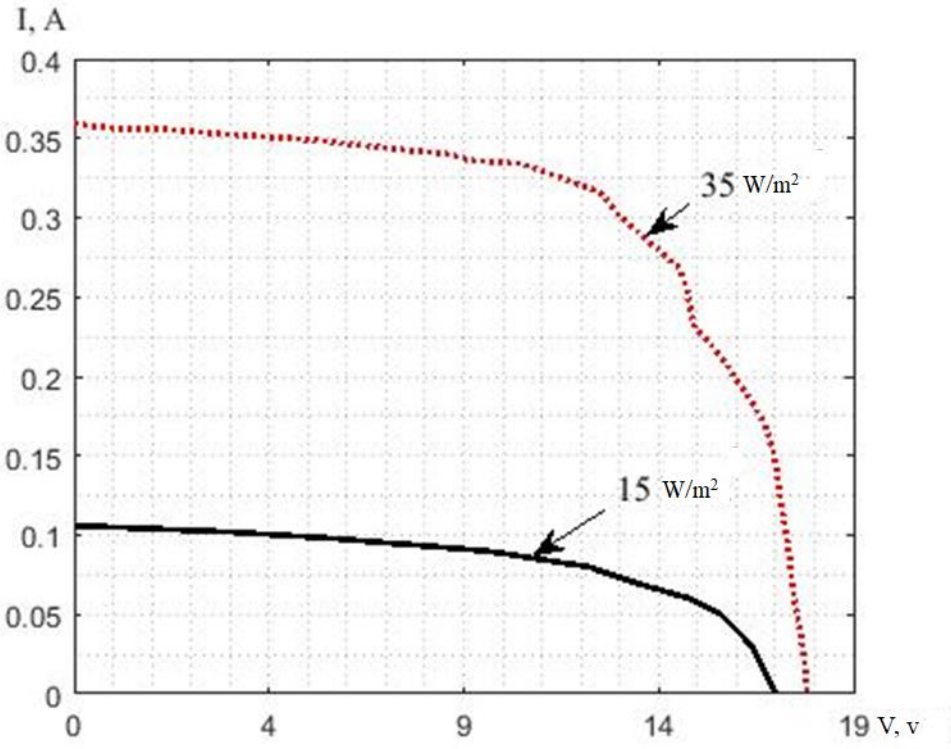

b)

Figure 2.4 − Light IVA of the ALM-50M solar battery at the radiation flux density: 1000, 700, 400, 200, 35 and 15 W/m ^{2}

(Where 1-6 is 1000-15 respectively)

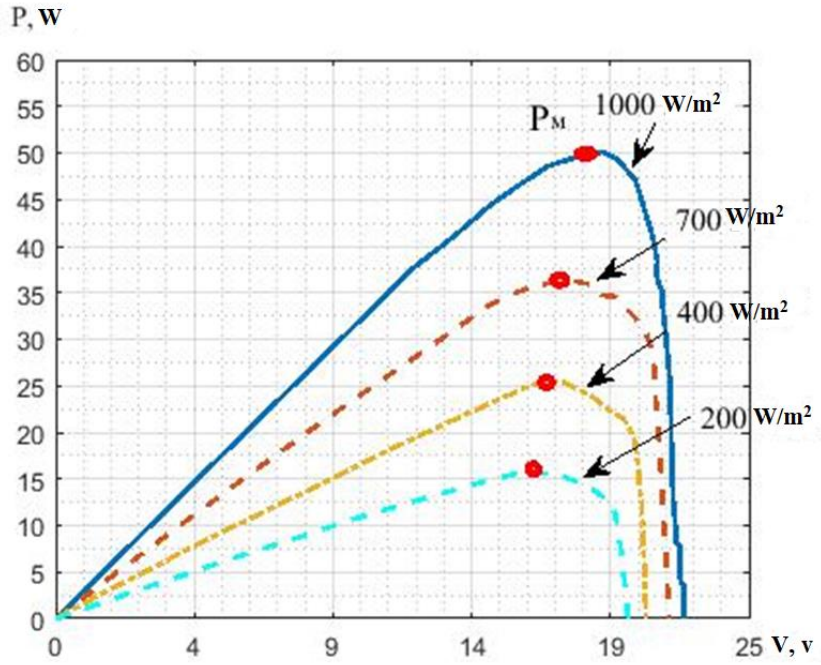

a)

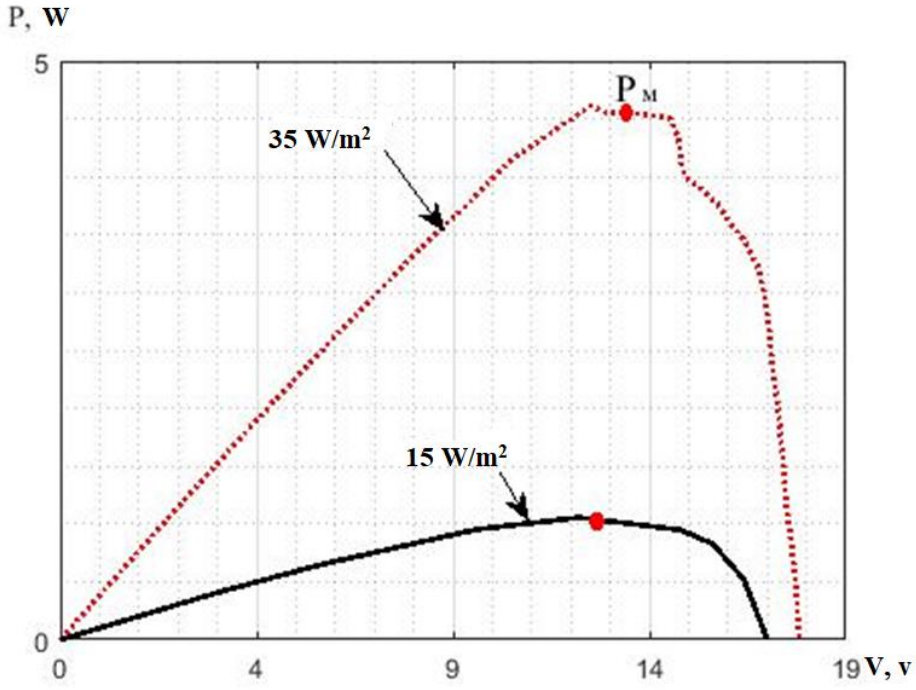

b)

Figure 2.5- Graph of the power change of the ALM-50M solar battery at the radiation flux density: 1000, 700, 400, 200, 35 and 15 W/m ^{2}

From these Figures, V_m, I_m, at which the maximum value of the consumed power, as well as the no-load voltage V_x and short circuit current I_x. These parameters are given in table 2.1. In addition, another parameter is introduced for solar cells, which is called the filling factor and is denoted FF and is determined from the equation FF= $V_m \cdot I_m / V_x \cdot I_x$. For this type of cell, this parameter is in the range of 0.44-0.75, which is somewhat underestimated for monocrystalline silicon cells. On the basis of the obtained I-V characteristics, the resistance values R_w and Rn, were calculated which are equal to 10.37 KOhm and 0.48 Ohm.

Table 2.1

	1000 *W/m²*	700 *W/m²*	400 *W/m²*	200 *W/m²*	35 *W/m²*	15 *W/m²*
R_n, *Ohm*	0.48	0.49	0.5	0.8	6.6	20
U_x, *V*	21.6	21.1	20.3	19.6	17.8	16.9
I_x, *A*	3.05	2.52	1.76	1.1	0.36	0.11

V_m, V	17.5	17.4	16.9	16.6	16.2	16.1
I_m, A	2.84	2.2	1.52	0.9	0.2	0.05
P_m, W	50	38	25	15	3	1
FF	0.75	0.72	0.72	0.69	0.5	0.44

The measurements of the dark current-voltage characteristics (IV curves) of the Schottky barrier (SB) were conducted in a dark room. The microammeter M 1109 was used to measure the current through the SB, and the power supply in this setup was a regulated voltage source of the LW-K3010D type, which provided a voltage resolution of 0.1V. The measurements of the dark IV curves were performed on the solar cells of the ALM-50M battery. Figure 2.6 shows the reverse branch of the dark IV curve of the ALM-50M solar cell. It can be divided into two regions with different slopes with respect to the voltage axis, corresponding to R1 = 10.37 kΩ and R2 = 8.32 kΩ, respectively. The reverse saturation current I0 = 400 μA was determined from the segment that intersects the current axis. These parameters were used in the modelling of the SB.

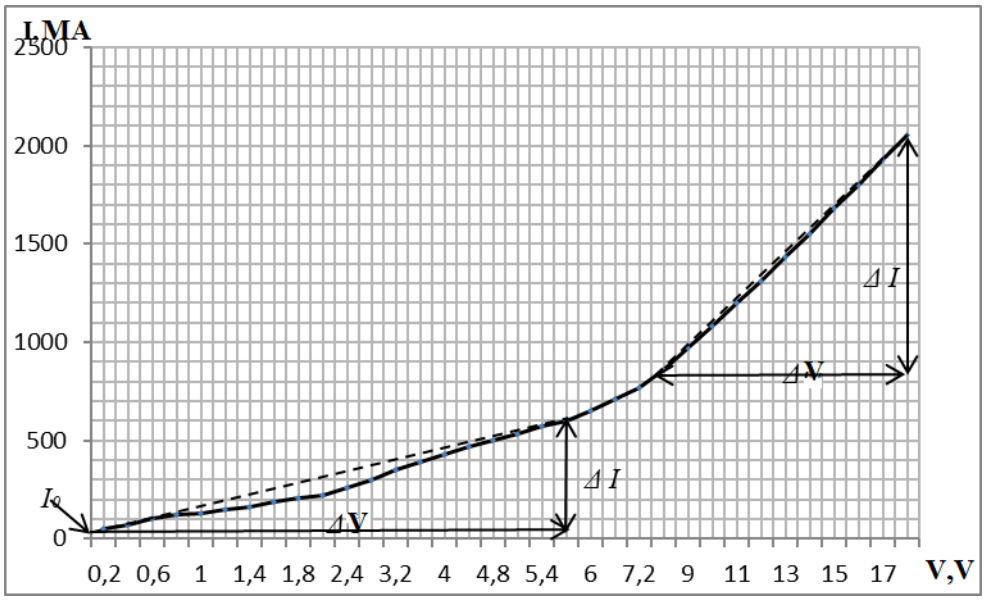

Figure 2.6- The reverse branch of the dark current-voltage characteristics (IV curve) of the ALM-50M solar cell.

The solar panel model ALM-50M was represented by an electrical circuit, as shown in Fig. 2.7, with corresponding nominal values of the components.

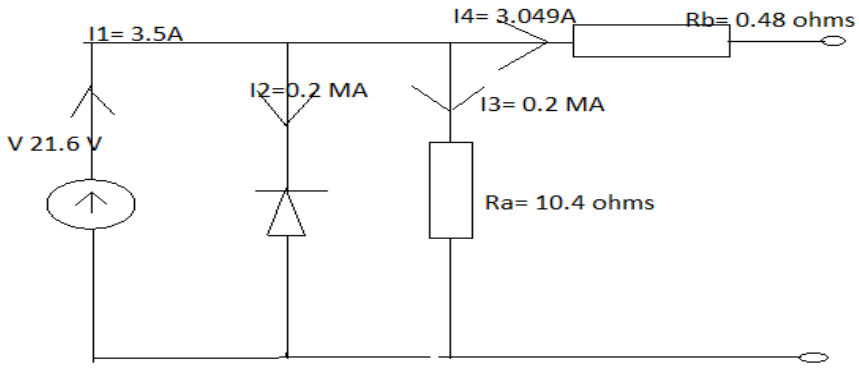

Figure 2.7- The electrical circuit of the solar panel model ALM-50M.

2.3. Construction of a PV Module-Load/Consumer Model

The electrical circuit used for constructing the PV module model is called the "single diode model". It consists of a current generator I_1, with a diode and a shunt resistor Ra connected in parallel to it. In series with the current generator, there is a resistor Rb. The equivalent circuit of the solar cell is shown in Figure 2.8.

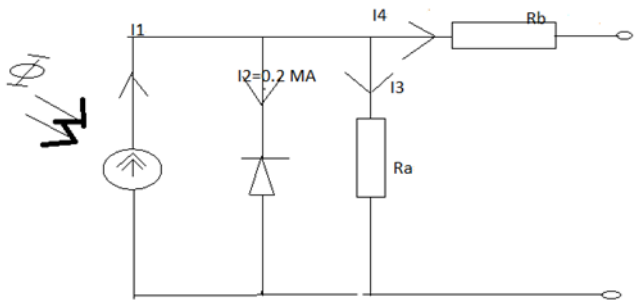

Figure 2.8- The equivalent circuit of a solar battery element.

Based on the fact that the current through the diode is described by the equation $I_2 = I_0\left(exp\frac{eV}{AkT} - 1\right)$and according to Kirchhoff's first law, the load current of the PV module can be written

$$I_4 = I_1 - I_0(\exp\frac{eV}{AkT} - 1) - \frac{V+I_4R_b}{Ra} \quad (2.1)$$

where V is the applied voltage;

I_0 – diode saturation current;

I_1 - photocurrent;

e – electron charge;

A is the coefficient of ideality ($1 \leq A \leq 2$);

k is the Boltzmann constant;

T is temperature.

Formula (2.2) is the most accurate for engineering calculations.

$$I_4 = I_1 - I_0(\exp\frac{eV}{AkT} - 1) \quad (2.2)$$

V_x and $I_{k.z}$ were also used, which were obtained on the basis of equation (2.4)

$$I_{к.z.} = I_f, \quad (2.3)$$

$$V_x = \frac{AkT}{e} ln\left(\frac{I_{k.z.}}{I_0} + 1\right). \quad (2.4)$$

When using solar panels as autonomous power sources for both lighting systems and other consumers, the task of calculating the conditions for the transmission of electricity to the consumer arises. The condition for transfer to the maximum power load is the condition when $R_a = R_b$. From the obtained values of the shunt resistance and the diode resistance, R_b was calculated, which was equal to 9.4 *kΩ*.

The efficiency coefficient η, which is determined by the ratio of useful power, or the power released in the load to the battery power and is equal to

$$\eta = \frac{P}{P_n} = \frac{R_1}{R_2+R_3}. \quad (2.5)$$

In the case of using centralized autonomous PV modules, from which it is necessary to transmit electricity through the power transmission line and to the consumer, the line resistance *R_3 is added to formula (2.6).*

$$\eta = \frac{P}{P_n} = \frac{R1+R3}{R1+R2+R3}. \quad (2.6)$$

Figure 2.9 shows the scheme of the solar energy system, which takes into account the resistance of the transmission line and the resistance of the load.

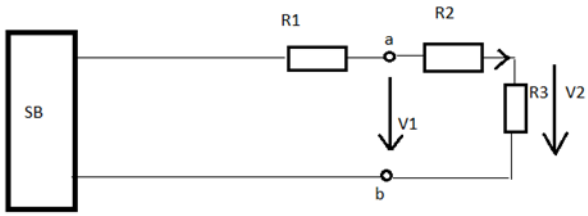

Figure 2.9- The equivalent circuit of the energy system consists of a solar battery (SB), a power transmission line, and a load (consumer).

2.4. Modeling the Characteristics of a Solar battery

The main elements of the circuit (Figure 2.8) are: current source, diode, parallel and series resistors. The current source models the process of generating photocurrent (I_1) in the element under illumination. The diode is connected in the forward direction parallel to the current source. Due to the presence of excess electron concentrations in the n-region of the element and excess hole concentrations in its p-region, caused by forward bias, a certain current (I2) flows through the diode. The shunt resistance of the photovoltaic cell, R1, arises due to the presence of the reverse resistance of the n-p junction and various conductive films or impurities on the surface of the element. It is also connected in parallel to the current source. The series resistance, R2, represents the resistance of the semiconductor material from which the photovoltaic cell is made. As seen from equations (2.2 and 2.4), the value of A affects Vx. Therefore, it is important to consider its value during modelling. Reducing the value of the diode's quality factor

significantly affects the voltage of the solar panel. Different values of the diode's quality factor result in deviations of the voltage from the nominal data shown in Figure 2.10. (Note that in the image A=n)

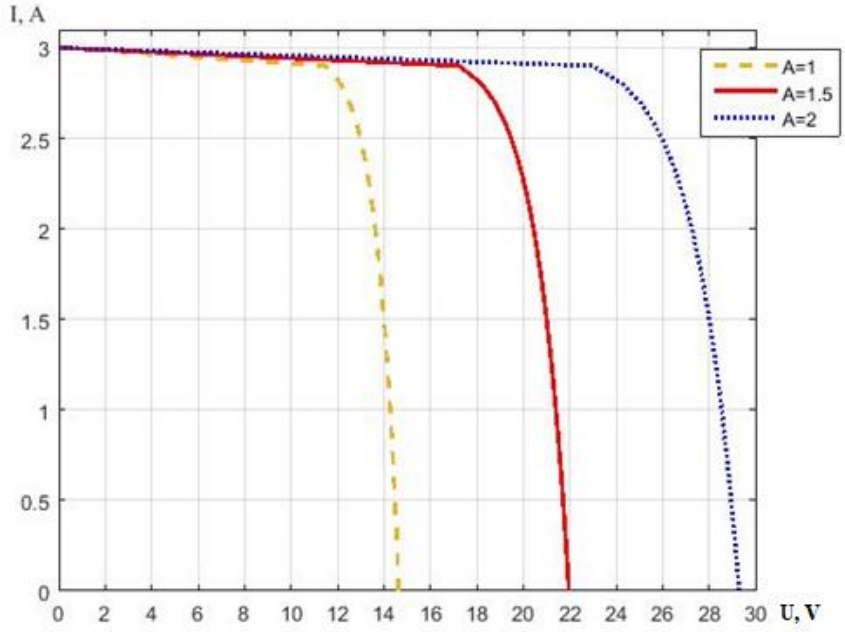

Figure 2.10 – The influence of the ideality factor of the diode on the I-V characteristic

The variation in the reverse saturation current of the diode significantly affects Vx. There can be cases where the reverse saturation current does not match in a batch of photovoltaic converters. This case was modeled and presented in fig. 2.11.

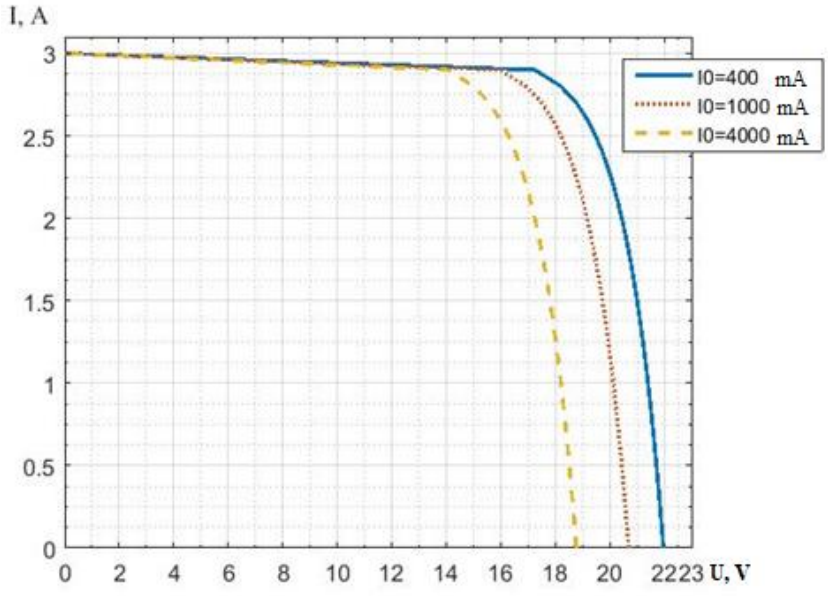

Figure 2.11 – The influence of the saturation current of the diode on the I-V characteristic

2.5 Schedule of Electricity Consumption in A Residential Building

A photovoltaic system for an autonomous residential house where 4 people reside permanently and the approximate daily energy consumption is almost 11 kWh (Table 2.2 and 2.3), thus the average power consumption amounts to 375 W.

Table 2.1. Daily electricity consumption in the cool season in a residential building (from 1 a.m. to 12 p.m.)

Consumer	**Power, *W***	**Number**	**Hours of energy consumption, *kW h***											
			1	2	3	4	5	6	7	8	9	10	11	12
Computer	100	1									0.1	0.1	0.1	
A single room	200	1	0.2	0.2	0.2	0.2	0.2	0.2	0.2	0.2	0.2	0.2	0.2	0.2
TV	50	1								0.05	0.05	0.05	0.05	0.05
LED lamps	40	2	0.04	0.04	0.04	0.04	0.04							
Lamps	20	2		0.02		0.02								
Kettle	1500	1						0.125				0.125		
Washing machine	1500	1												1.5
Water pump	370	1								0.28				
		W	0.24	0.26	0.24	0.26	0.24	0.325	0.2	0.53	0.35	0.475	0.35	1.75

Table 2.2. Daily electricity consumption for the cool season in a residential building (from 13 to 24 hours)

Consumer	**Power, *W***	**Number**	**Hours of energy consumption *kW h***											
			13	14	15	16	17	18	19	20	21	22	23	24
Computer	100	1		0.1	0.1	0.1				0.1	0.1			
Refrigerator	200	1	0.2	0.2	0.2	0.2	0.2	0.2	0.2	0.2	0.2	0.2	0.2	0.2
Tele viewfinder	50	1						0.05 _			0.05 _	0.05		
LED lamps	40	2							0.08	0.08	0.08	0.08	0.08	0.08
Lamps	20	2						0.04	0.04	0.04	0.04	0.04	0.04	0.04
Kettle	1500	1			0.125									
Washing machine	1500	1				1.5								
Water pump	370	1		0.185										
		W	0.2	0.485	0.425	1.8	0.2	0.29	0.32	0.42	0.47	0.37	0.32	0.32

(The total energy consumption per day is 10.84 kWh)

In fig. 2.12 and 2.13 graphically present the data of the table. 2.2 and 2.3

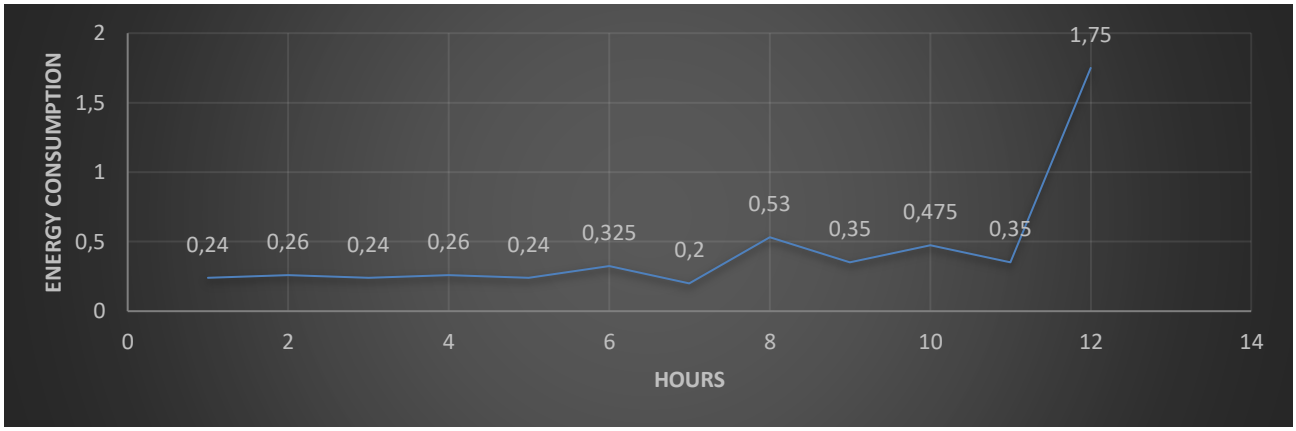

Figure 2.12- Energy consumption per hour from 1 to 12 according to the table 2.2

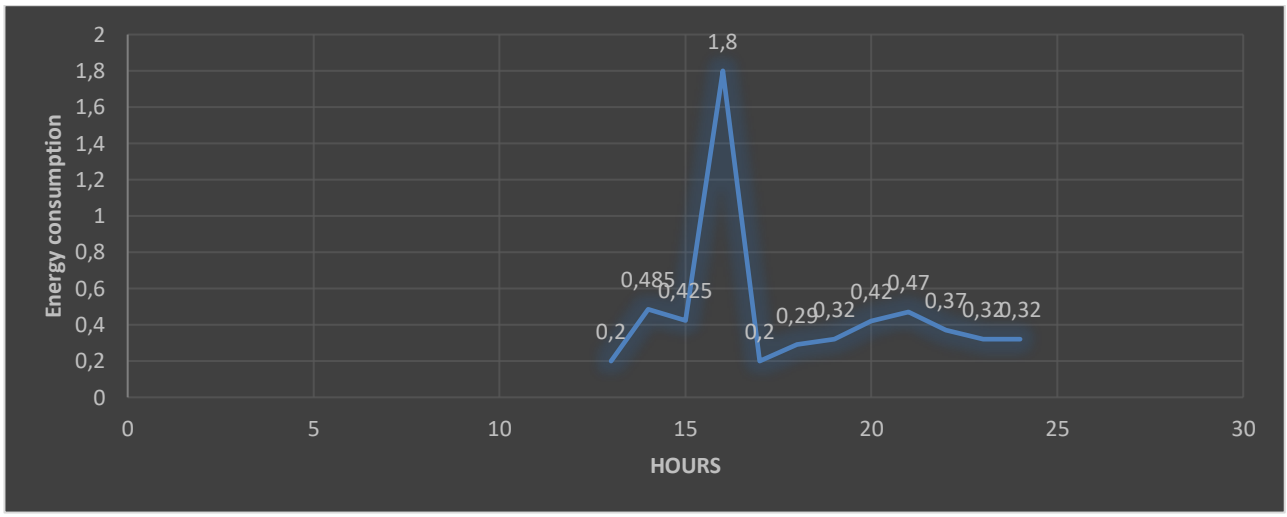

Figure 2.13- Energy consumption per hour from 13 to 24 according to the table 2.3

Total energy in kilowatt-hours per night (tables 2.2 and 2.3)

$$\Sigma W_{\text{n}} = W_{19} + W_{20} + W_{21} + W_{22} + W_{23} + W_{24} + W_1 + W_2 + W_3 + W_4 + W_5 + W_6$$
$$= 0.32 + 0.42 + 0.47 + 0.37 + 0.32 + 0.32 + 0.24 + 0.26 + 0.24 + 0.26 + 0.24 + 0.325$$
$$= 3.8kWh$$

The total energy in kilowatt-hours per daylight

$$\Sigma W_{\text{day}} = W_7 + W_8 + W_9 + W_{10} + W_{11} + W_{12} + W_{13} + W_{14} + W_{15} + W_{16} + W_{17} + W_{18}$$
$$= 0.2 + 0.53 + 0.35 + 0.475 + 0.35 + 1.75 + 0.2 + 0.485 + 0.425 + 1.8 + 0.2 + 0.29$$
$$= 7.05\ kWh$$

Total energy consumption per day,

$$\Sigma W_{\text{cons}} = \Sigma W_{\text{day}} + \Sigma W_{\text{night}} = 7.05kWh + 3.8kWh = 10.85kWh$$

Average power for the night (Figure 5) P $_{\text{avg. night}}$

$$P_{\text{avg.night}} = \frac{\Sigma W_{\text{night}}}{T_{\text{night}}} = \frac{3.8kWh}{12h} = 0.3kW \quad (2.7)$$

Average power per daylight

$$P_{avg.\text{ day}} = \frac{\Sigma W_{\text{day}}}{T_{\text{day}}} = \frac{7.05kWh}{12h} = 0.6kW \quad (2.8)$$

In Figure 2.14 shows the graph of power consumption, the peak of which reaches 1.8 kW due to the inclusion of the washing machine. Energy consumption in residential buildings is almost constant throughout the year. In the evening and at night there is a maximum energy consumption.

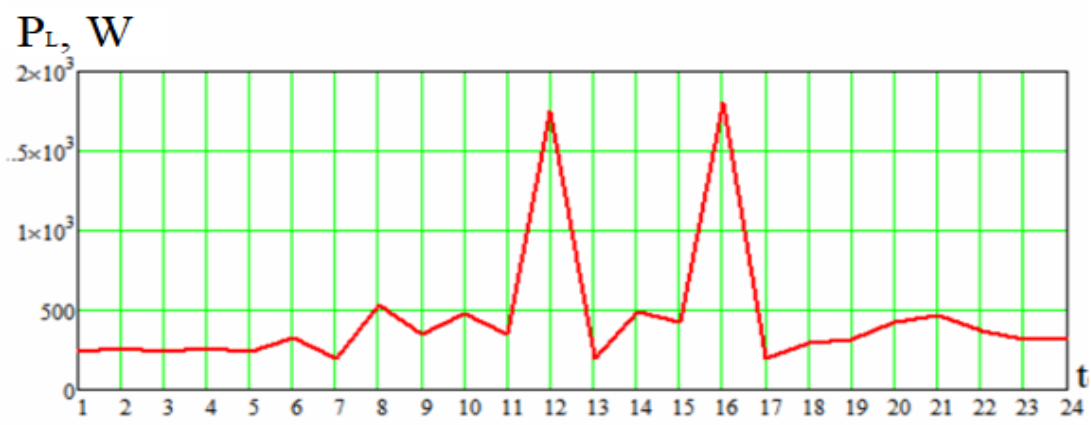

Figure 2.14 - Cyclogram of consumed power from 1 to 24 hours

2.6 Selection of Accumulator Battery Type and Its Maintenance System

The next task is the selection of the accumulator battery type. Next, we will consider the extended characteristics of batteries that allow for a justified selection of battery types based on statistical analysis:

- The internal resistance of the battery depends on the internal resistance of each of its elements, the type of protection circuit, and the number of elements in the battery. The protection circuit of lithium-ion and lithium-polymer batteries increases their internal resistance on average by 100 mΩ (0.1 Ω).

- The service life of the battery depends on the regularity of its maintenance and the use of charge-discharge cycles, including full periodic discharge and charge.

- The service life also depends on the depth of discharge - it is longer for partial discharges compared to full discharges.

- Nickel-cadmium and nickel-metal hydride batteries allow for immediate maximum discharge current after charging. Nickel-cadmium batteries lose 10% of their capacity within the first 24 hours after charging due to self-discharge, followed by a decrease in capacity of approximately 10% every 30 days. Self-discharge increases with rising temperature.

- The protection circuit installed inside lithium-ion and lithium-polymer batteries consume approximately 3% of their energy per month. The typical voltage value for nickel-cadmium and nickel-metal hydride batteries is 1.25 V in idle mode and 1.2 V under load.

- Acid batteries can be charged with strong current impulses.

- Nickel-cadmium batteries have the shortest charging time, allow for the highest load current, and have the lowest price-to-service-life ratio. However, they are also the most critical in terms of strict adherence to proper operation requirements.

Among the known battery types for the photovoltaic system, lead-acid and gel batteries are most commonly used. We choose gel batteries due to their unique characteristics, including the absence of a charge current regulator, a high number of charge-discharge cycles, tolerance for prolonged discharge, low self-discharge, and the ability to operate in any position in a residential space. Gel batteries are widely used in electric transportation, powerful home backup power systems, and alternative energy applications. The rapid advancement of polymer battery technologies is likely to displace gel batteries in small and medium capacities. However, for large capacities (100 Ah and above), lead-acid batteries are expected to dominate for a long time. Gel batteries require protection against overcharging and should have a voltage limiter during charging to ensure a maximum service life of over 700 charge-discharge cycles.

Advantages of gel batteries include:

- No maintenance is required.

- They can be transported by air.

- They are spill-proof and leak-proof.

- They are corrosion-resistant.

• They have high performance during deep discharge.

• They can be installed on their side (with a possible 10% power loss).

• They do not emit gas.

• They can be used alongside sensitive electronic equipment.

• They have a long storage life and can withstand prolonged storage.

• They recharge faster (0% to 90% in 3.5 hours) - 7 times faster than equivalent acid batteries.

• There is no current limitation during charging up to 13.8V.

• They are vibration-resistant.

• They offer increased safety at sea as they do not produce gas in the hold (from the interaction of sulfuric acid and saltwater).

• They are versatile and can be used as starter batteries, deep-cycle batteries, or stationary batteries.

• They can operate in wet environments, even at depths of up to 10 meters underwater.

• They do not freeze at temperatures as low as -20 °F / -30 °C when fully charged.

• Optimal specific cost (price / number of months in service).

• Lowest specific cost (price / number of cycles).

Characteristics of gel batteries:

• Higher initial cost.

• Higher weight compared to other batteries.

• It is not possible to add water during prolonged overcharging.

• It requires the use of temperature-sensitive, regulated voltage chargers, which should be limited to maintain the battery's service life at a level of 13.8-14.1V maximum at 20°C.

2.7 The Choice of Design and Voltage for An Autonomous Photovoltaic System

Since a sun-tracking system with solar panels directly facing the sun requires complex automated electrical control, a fixed solar panel with a selected tilt angle $\beta = 40°$, located

on the roof and parallelly connected to the battery bank (AB), is used according. As the consumers require a standard voltage of 220 V with a frequency of 50 Hz, a boost stabilizing voltage inverter with a sinusoidal waveform will be used between the battery bank and the consumer. During the nighttime, the inverter will be powered by the battery bank, which gets charged during the day. The choice of voltage for the solar panel and the battery bank is made considering the following considerations:

1. Ensuring the safety of the solar panel and battery bank, which decreases with increasing voltage.

2. Achieving reliability of the battery bank and solar panel. Reliability decreases in high-voltage schemes with 220 V.

3. High-voltage battery banks have a large voltage spread between battery elements and require a complex balancing system to prevent failure.

4. The most common battery bank configuration is a sealed lead-acid battery (with absorbed electrolyte or gel) used in automobiles, with a voltage range of 10 to 14 V.

The determination of the specific voltages for the battery bank and solar panel will be made after studying various converter schemes within the range of 10 to 220 V with a sinusoidal (AC) output voltage.

2.8 Analysis of The Traditional Structure of An Autonomous Photovoltaic System.

Figure 2.15 shows the structure of a photovoltaic system with a current source PV1 simulating a solar panel, a battery bank (AB), and an inverter with a step-up transformer TV. The battery bank starts charging when the voltage of the solar panel increases due to the rising illumination, reaching the minimum voltage level of the battery bank, which is around 10 to 12 V. Let's determine whether a boost voltage invert L2, VT3, VD6 is required between the solar panel and the battery bank (Figure 2.15). There are possibilities for aligning the energy characteristics of the system components considering the external conditions. These are typical characteristics of the solar panel current I_{SP} (A), solar panel voltage V_{SP} (V), ambient temperature variation T(°C), and

solar radiation power variation throughout the day P_C (W/m^2). It can be observed that energy deficiency from the solar panel occurs from 6 to 7 in the morning and from 17 to 18 in the evening when $V_{SP} < V_{AB}$.

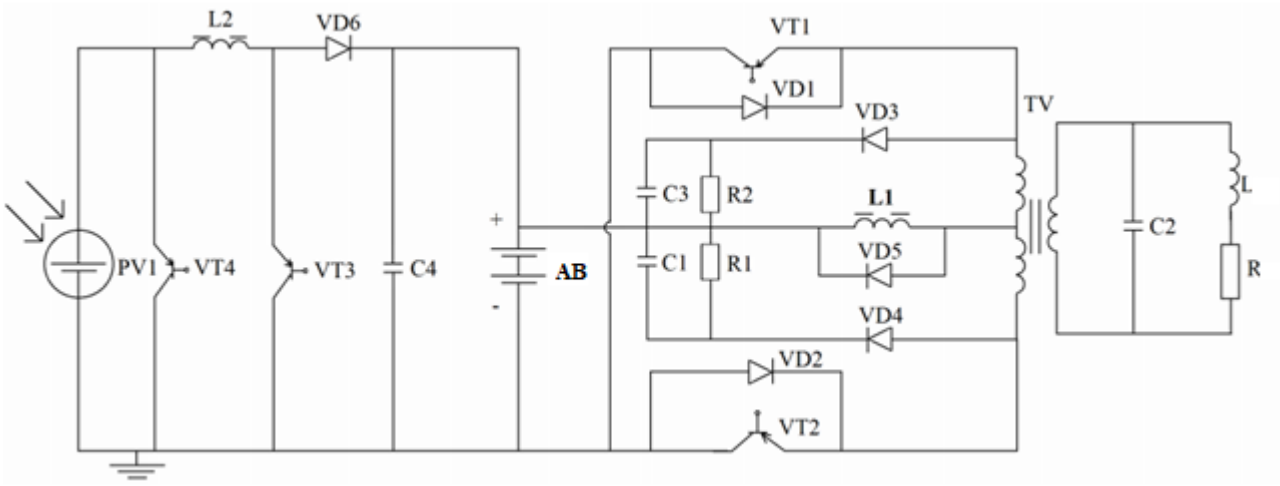

Figure 2.15- The circuit diagram of a photovoltaic system with a battery modelled as a controlled current source PV1 and a voltage-boosting converter consisting of L2, VT3, and VD6 to increase the voltage of the solar battery.

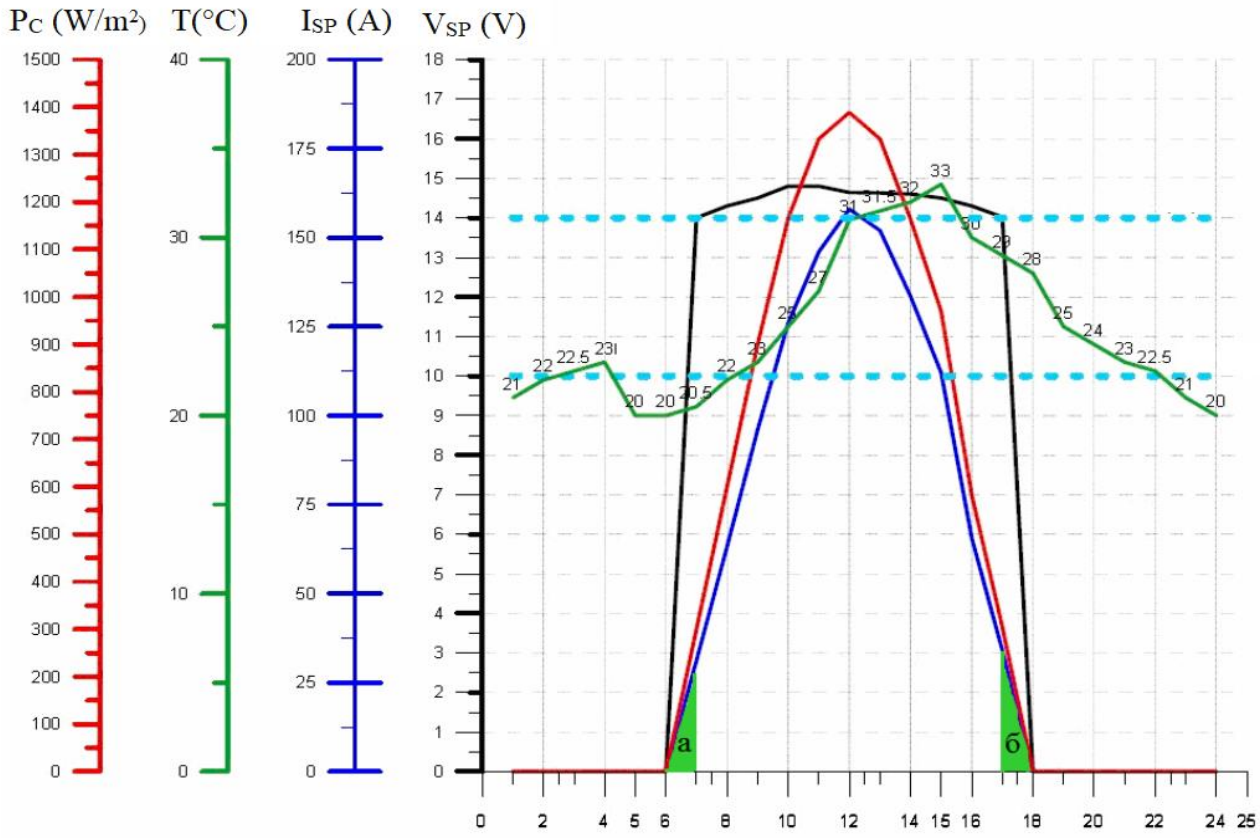

Figure 2.16 - Coordination of SB characteristics with battery voltage depending on the illumination by the Sun

Let's calculate the maximum charge that can be delivered by the solar module (SB) theoretically during the period of illumination:

$$Q_{\text{max. SB}} = I_{\text{avg.SB}}\, t_s = 70 \cdot 12 = 840Ah \quad (2.9)$$

Next, let's calculate the charge loss ΔQ when $V_{SB} < V_{AB}$. This occurs twice a day for one hour each time:

$$\Delta Q_1 = \frac{I_{\text{max. }\Delta} t_\Delta}{2} = \frac{50A*1h}{2} = 25\text{Ah} = \Delta Q_2 \quad (2.10)$$

where I_max,Δ is the maximum current through the solar module one hour after the start of illumination, and t_Δ is the time when $V_{SB} < V_{AB}$.

Now, let's calculate the total charge loss due to $V_{SB} < V_{AB}$:

$$\Sigma_\Delta Q = \Delta Q_1 + \Delta Q_2 = 25 + 25 = 50\text{A}h \quad (2.11)$$

Finally, we can calculate the relative charge loss without the inverter:

$$\xi = \frac{\Sigma_\Delta Q}{Q_{max.SB}} = \frac{50}{2475} = 0.02 = 2\%. \quad (2.12)$$

where ζ represents the fraction of capacity loss.

In this case, considering a 2% loss, there is no significant need to use voltage boosting. The analysed systems in Section 4 did not utilize this converter because the calculations showed that it did not provide benefits when considering a converter efficiency of 0.8. It has been proven that it is possible to create a photovoltaic system without a voltage inverter between the SB and the battery (AB). The converter with L2, VT3, and VD6 (Fig. 2.15), which boosts the voltage, has an efficiency of 0.8. Its inclusion allows for the utilization of energy for charging the battery from 6 to 7 in the morning and from 17 to 18 in the evening. However, the losses in the boosting inverter L2, VT3, and VD6 compared to the additional energy led us to choose the parallel

connection of the solar module and accumulator the battery pack (B) through diode VD6, eliminating the need for L2 and VT3.

2.8.1 Synthesized structure of an autonomous photovoltaic installation

Photoelectric power plant for a cottage, taking into account the analysis of the elements, contains a primary source - a solar battery (SB) (Fig. 2.17), placed on the roof and constantly oriented to the south with a selected angle of inclination β = 40˚, a battery and a protection unit and an inverter of constant voltage to alternating voltage . The task of the study was to determine the optimal voltage AB and SB, type of voltage converter at fixed load parameters. It is necessary to analyze a PV module with a voltage of AB and SB between 14 V and 220 V with an inverter to an alternating voltage of 220 V with a frequency of 50 Hz and a sinusoidal shape with a distortion of less than Kg (UH) ≤ 10%. AB protection against overvoltage is provided by the "AB protection block".

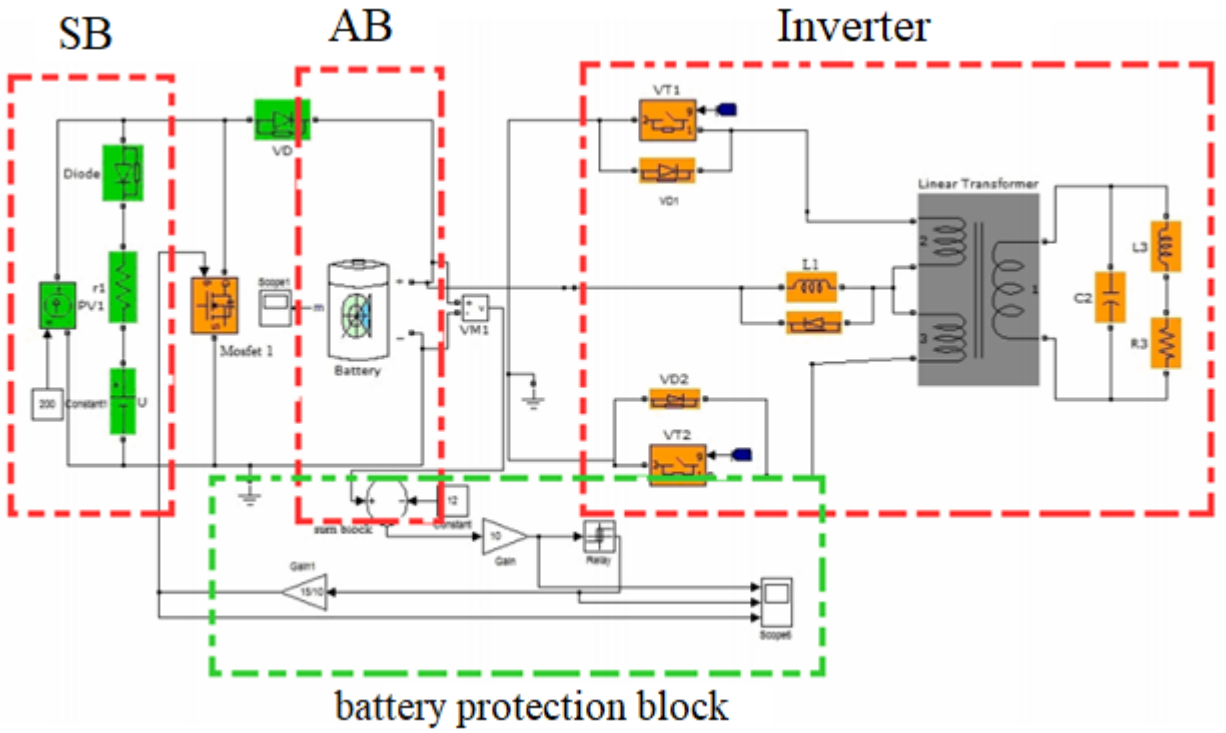

Figure 2.17 - The investigated structural diagram of the photoelectric power plant in Simulink.

2.9 Conclusions For This Section:

1. A methodology has been developed, and an experimental setup has been constructed to measure the light and dark current-voltage characteristics of photovoltaic cells (PVCs), determine the maximum power current and voltage, and measure the reverse saturation current of the p-n junction.

2. For the construction of the PVC model, a "single-diode model" has been proposed.

3. The influence of the diode ideality factor and reverse saturation current on Vx has been simulated. It has been shown that increasing the reverse saturation current from I0=400 mA to I0=4000 mA leads to a decrease in Vx from 21.6 V to 19 V, which in turn reduces the output power.

4. The selected structure of the photovoltaic system is based on a simple protection and control scheme for the battery without a voltage-boosting inverter between the solar battery and the battery. The solar battery is installed on the roof with an inclination angle of $\beta = 40°$, protects against rain. Installing the solar battery on the roof enables the use of solar energy in remote areas.

5. It has been proven that it is possible to create a photovoltaic system without a voltage inverter between the solar module and the battery, which is relevant.

6. Based on statistical analysis, a gel battery has been chosen from 7 types of batteries based on the criteria of maintenance-free operation and maximum energy density of up to 180 W/kg. The chosen method for protecting the battery from overvoltage is by short-circuiting the solar battery.

3. CALCULATION SECTION

3.1 . Energy Balance of Photovoltaic System

The energy balance is conducted for daily consumption according to tables 2.2 and 2.3. The solar battery (SB) starts charging the battery AB, when the illumination increases and voltage ($V_{X,sb}$) of the solar module becomes greater than voltage of the accumulator battery $V_{AB,min}$. During the battery charging process, the operating point (Figure 3.1) moves from point 2 to point 1.

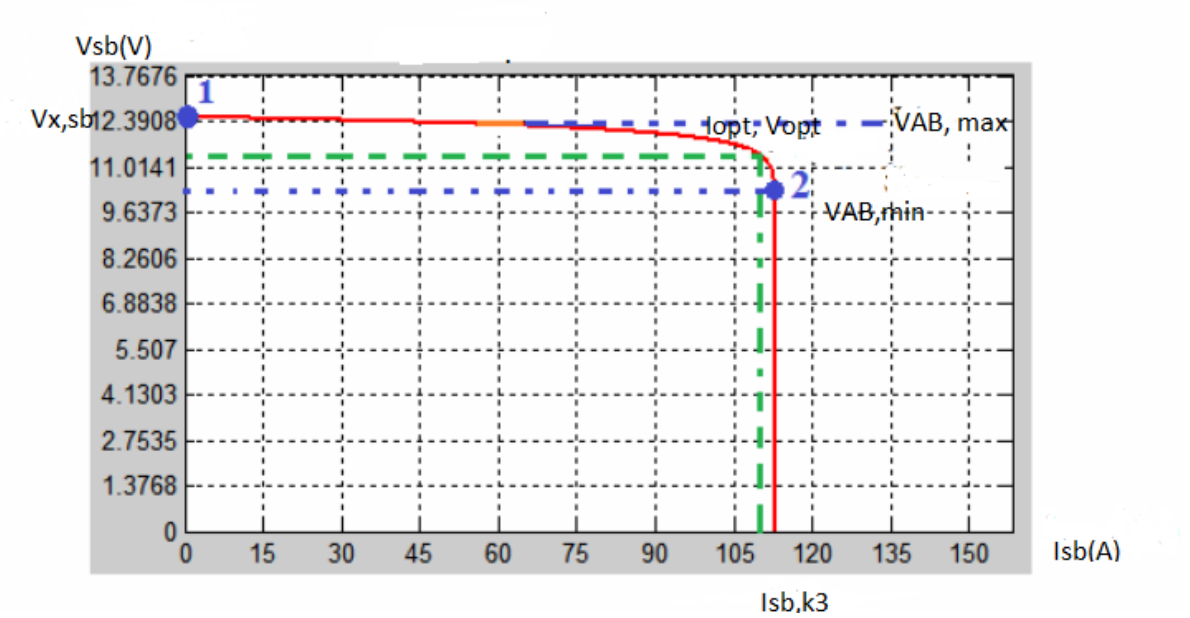

Figure 3.1- Matching the characteristics of the solar battery (SB) and the accumulator battery (AB).

In this case, the charging current of the accumulator (AB) decreases from the value of I_{K3} to the optimal value of Iopt and further decreases to zero at point 1, where Vx,SB = Vmax,AB. In this project, the photovoltaic system operates with a limitation on the accumulator battery voltage (AB). At the discharge voltage of AB, VAB = 12 V, the average discharge current of AB I_{dsc}, once, night (A) is calculated as:

$$I_{\text{dsc, night time}} = \frac{P_{dsc,\,\text{night}}}{V_{AB}} = \frac{0.3kVm}{12V} = 25A \qquad (3.1)$$

The average discharge current for the load during the day (Figure 3.2) is I_{dsc}, once, day:

$$I_{\text{dsc, day}} = \frac{P_{dsc,day}}{\text{V}} = \frac{0.6kVm}{12V\text{AB}} = 50\ \text{A} \qquad (3.2)$$

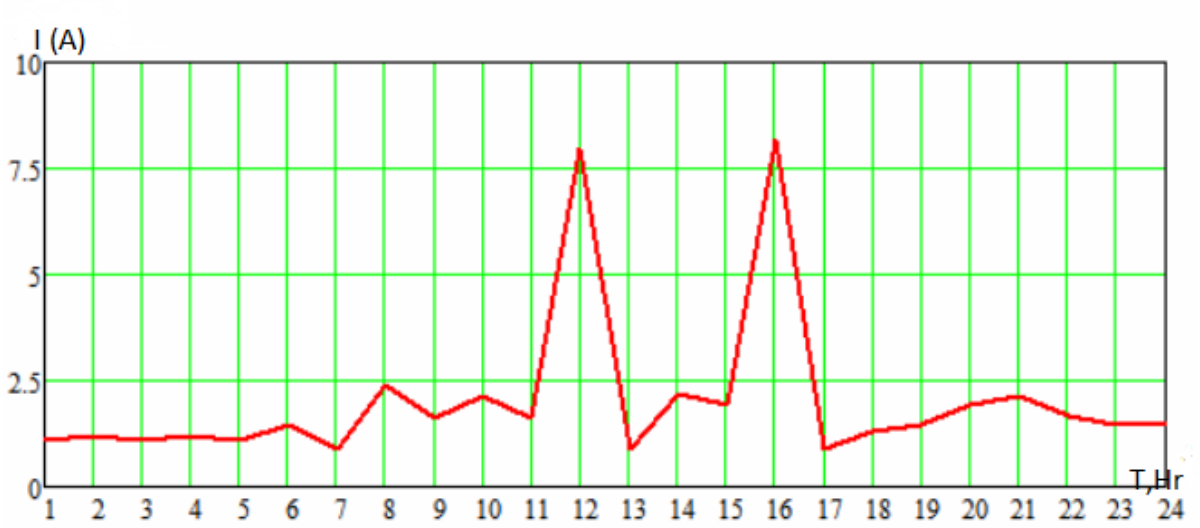

Figure 3.2- Load current cycle

The efficiency of lead-acid batteries discharge, η = 0.85. The discharge capacity of AB for night time exposure, QAB, once, night (I,A·T,h) taking into account the discharge efficiency and $T_{night} = T_{day} = 12$ hours is:

$$Q_{AB,night} = \frac{I_{dsc,night} * T_{\text{night}}}{\eta_{\text{discharge}}} = \frac{25A*12h}{0.85} = 352.94 \qquad (3.3)$$

The discharge capacity of AB for load during the day QAB, once, day (I,A·T,h) is:

$$Q_{AB,day} = I_{dsc,day} * T_{\text{day}} = 50A * 12h = 600 \qquad (3.4)$$

The average value of the solar module current I_{dsc}, SB (A) is:

$$I_{dsc,SB} = \frac{\Sigma Q_{SB}}{T_{\text{day}}} = \frac{953\text{Ah}}{12h} = 79\ \text{A} \qquad (3.5)$$

The maximum value of the solar battery current is determined by the size of the for stationary SB, and the average value of the current varies according to a sinusoidal law:

$$I_{\text{dsc, SB}} = \frac{2}{\pi} * I_{\text{max, SB}} = 0.64\ I_{\text{max, SB}}(A) \qquad (3.6)$$

From equation (3.7), we determine the maximum current of the battery: neglecting energy losses when $U_{SB} < U_{AB}$:

$$I_{\text{max, SB}} = \frac{I_{dsc,SB}}{0.64} = \frac{79A}{0.64} = 123A \quad (3.7)$$

3.2 Calculation of the area of the solar battery

The maximum specific power delivered by the solar panel to the battery with C-Si PV module (W/m^2) is:

$$P_{SB} = \text{P} * \eta = 1000\frac{Vm}{m^2} * 0.24 = 240\frac{Vm}{m^2} \quad (3.8)$$

The average specific power of the solar panel P_{SBs} is calculated as:

$$P_{SBs} = P_{SB} * \frac{t_{\text{day}}}{t_{\text{day}} + t_{\text{night}}} = 240\frac{Vm}{m^2} * \frac{12h}{24h} = 120\frac{\text{Vm}}{m^2} \quad (3.9)$$

The average load power P_{NS} (W) over 24 hours is:

$$P_{NS} = P_{\text{dsc, night}} + P_{\text{dsc, day}} = 0.3kVm + 0.6kVm = 0.9kVm \quad (3.10)$$

From the equality of average load power and average specific power of the solar panel, we calculate the area of the solar panel S_{SB}:

$$S_{SB} = \frac{P_{Ns}}{P_{SBs}} = \frac{900}{120}\frac{Vm}{\text{Vm/m}^2} = 7.5\text{m}^2 \quad (3.11)$$

3.3. Calculation of The Operating Cyclic Capacity of the Accumulator Battery

To construct the cyclic capacity profile Qc, we first need to calculate the charging and discharging capacities: + QAB - charging capacity of AB, and - QAB - discharging capacity of AB (Table 3.1). Let's calculate the hourly increase in charging and discharging capacities of accumulator (AB):

Table 3.1. Calculation of charging and discharging capacity of AB

Time (h)	Releasable charge SB, Q_{SB} ($A \cdot h$)	The charge received by the load, Q_H ($A \cdot h$) (At AB = 12 V)	AB charging and discharging capacities (Increase)	AB capacity, Q_{AB} ($A \cdot h$) (Actual)
1	0	20	-20	201
2	0	21.7	-21.7	179
3	0	20	-20	159
4	0	21.7	-21.7	137
5	0	20	-20	117
6	0	27.1	-27.1	90
7	40.8	16.7	24.1	*24*
8	61.7	44.2	17.5	42
9	83	29.2	53.8	96
10	105	39.6	65.4	161
11	127	29.2	97.8	259
12	142	146	-4	255
13	131	16.7	114.3	369
14	109	40.4	68.6	438
15	88	35.4	52.6	***490***
16	42	16.7	25.3	430
17	0	24.2	-24.2	406
18	0	26.7	-26.7	379
19	0	35	-35	344
20	0	39.2	-39.2	305
21	0	30.8	-30.8	274
22	0	26.7	-26.7	248
23	0	26.7	-26.7	221
24	42	16.7	25.3	430

Let's calculate the cycling capacity with the minimum battery capacity of 24 $A \cdot h$ and the maximum battery capacity of 490 $A \cdot h$ (Table 3.1).

We obtain the cycled capacity Q_c

$$Q_c = \Delta Q_{AB} = Q_{max} - Q_{min} = 490 - 24 = 466 \approx 470 \quad (3.12)$$

To ensure a long service life, the charge-discharge cycle of ordinary AGM batteries should be less than 30% of the nominal capacity of the battery, and gel batteries allow up to 80% of the charge-discharge cycles of the nominal capacity according to this project. To increase the service life of the battery, we set the charge-discharge cycle $Q_c = 0.5 \cdot Q_c(A \cdot h)$.

Let's calculate the nominal capacity of AB:

$$Q_n = 2 \cdot Q_n = 2 \cdot 470 = 940 \approx 1000 \quad (3.13)$$

The calculated capacity $Q_H = 1000\ A \cdot h$ allows you to increase the service life of the battery due to the fact that this capacity provides up to 50% of charge-discharge cycles, which is shown in the cycle diagram of the AB capacity (Fig. 3.3), although according to the technical parameters, these batteries allow up to 80 % of charge-discharge cycles from the nominal capacity.

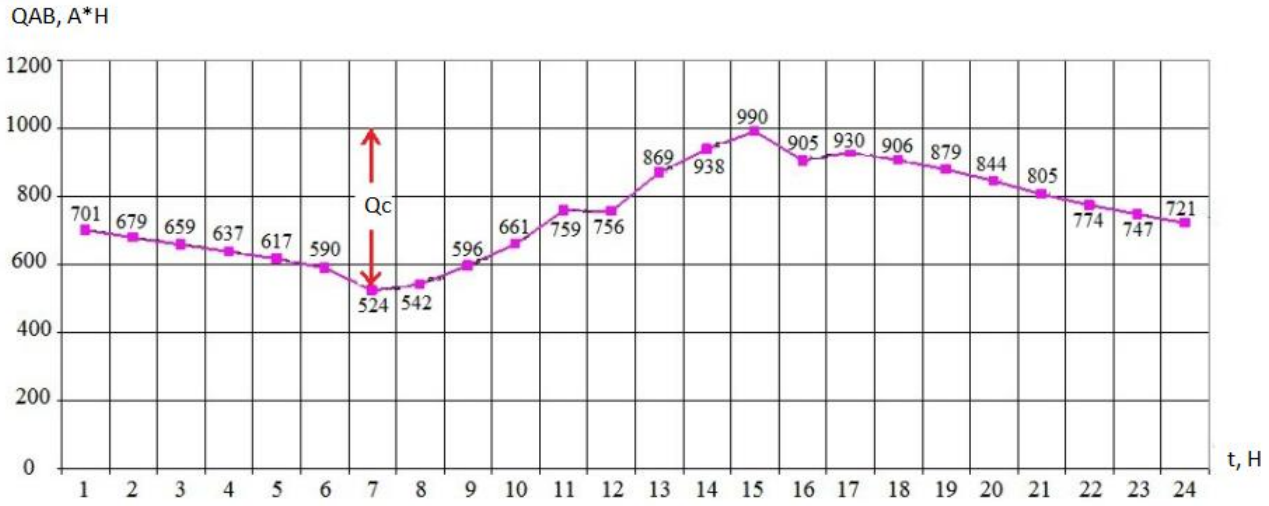

Figure 3.3- Battery Capacity Profile

3.4 . The Main Objectives in Creating a Photovoltaic System

1. Selection of AB and SB voltage (low voltage or high voltage variant) based on the following criteria: absence of overvoltage, transformer dimensions, magnitude of reverse current through diodes, SB voltage taking into account its location on the roof of the building to ensure safety, and the shape of the output voltage. Six different inverter circuit variants were investigated.

2. Calculation of inverter parameters and technical-economic characteristics. AB and SB voltage were selected between 14 V and 220 V, and inverted to standard 220 V AC with a frequency of 50 Hz and a sinusoidal waveform with distortion less than K^g (V_H) ≤ 10%. The results of modeling in the MATLAB-Simulink environment with different nominal voltages and types of inverters allow for the selection of AB and SB voltage. The SB model consists of a controlled current source PV1 (Fig.3.4) connected to AB through a blocking diode VD.

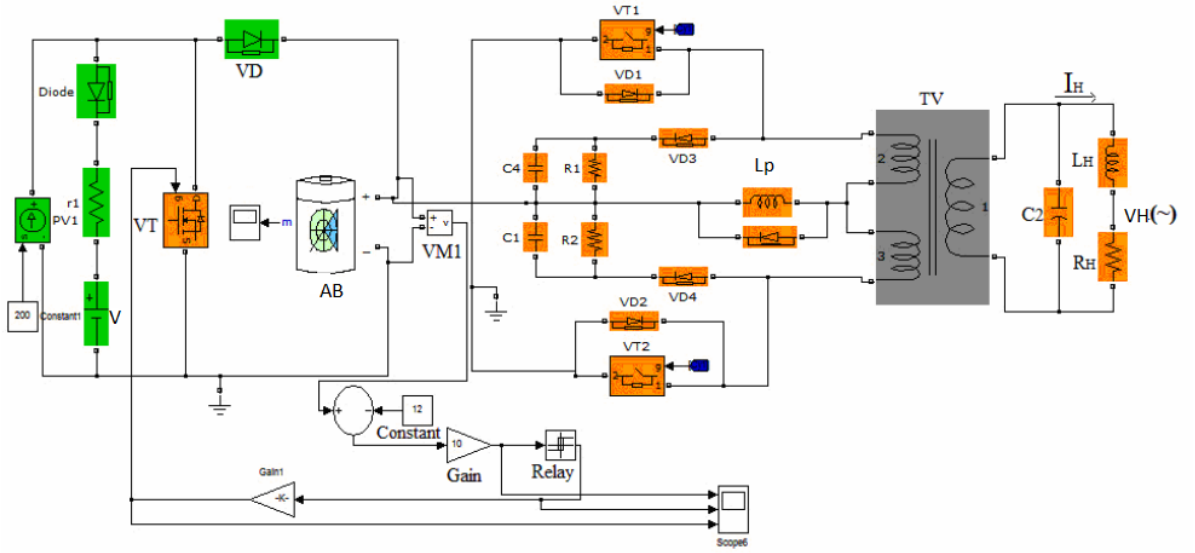

Figure 3.4- Simulation model in Simulink

The charging circuit (AB) is connected to PV1. In the AB circuit, it is necessary to include a controller VM1 (Gain, Relay) to prevent overcharging of AB. When the solar module charges the accumulator to the desired maximum voltage, the charging circuit parallel to the solar panel connects a charging transistor VT to absorb the excess power from the solar panel. AB is protected against overcharging by a relay regulator, which includes a reference voltage sensor (Constant), a voltage comparator device Battery (Constant) - sum block, an error amplifier of the controller (Gain), and a relay block (Relay) that controls VT. When the charging voltage on AB reaches 14 V, SB is short-circuited by the VT switch.

To match the characteristics of SB and AB, the SB voltage at the maximum power point is selected to be equal to the maximum charging voltage of AB, which is 14 V. The simulation step size was chosen to be 2×10^{-5} s. In the low-voltage scheme with V_{AB} = 10 - 14 V, a power transformer (TV) is used to increase the voltage to VH = 220 V. The transformation ratio of the transformer is represented by the coefficient. An

inverter with a square waveform output and voltage regulation at a frequency of 50 Hz using Pulse Width Modulation (PWM) was investigated. The sinusoidal waveform at the load is achieved by a parallel resonant LC circuit connected to the inverter through the transformer TV. The inductance LP smoothens the inverter's current consumption. The inductance LH of the active-inductive load with cosφ = 0.8 and the parallel-connected transformer TV with capacitor C2 form a parallel resonant circuit. The load is connected to capacitor C2 and has a sinusoidal waveform with distortion K_g(VH) ≤ 10%. When selecting VAB = 220 V, the power transformer TV, which increases the voltage from 14 V to 220 V, is not present. Control pulses for the power transistors are generated in such a way as to approach the waveform of the output voltage and current to a sinusoidal form in the most economical way. This is most commonly recommended for systems powered by renewable energy sources.

3.5 Study of Various Options of Inverter Schemes

The research investigated six different configurations (Fig. 3.5 to 3.10) of inverters with high-voltage and low-voltage input voltages, using two methods of connecting the smoothing choke: in the DC bus and in the AC bus. Two power circuit configurations were considered: the center-tapped power transformer scheme and the bridge scheme with a linear (ideal) transformer. The study examined various voltage levels for the DC link and AC bus with a recommended consumer operation algorithm. To limit the overvoltage in the DC bus, diode D1 is shunted across choke L1 (Fig. 3.5). The research revealed that in the low-voltage configuration, the inductance L2 (Fig. 3.6) in the AC current path should be four times greater than in the DC bus. This is due to the high voltage of 220V being applied to the output AC choke. In the high-voltage configuration, the inductance L1 (Fig. 3.7) in the DC bus is 30 times greater than in the AC bus, which necessitates the inclusion of an additional parallel choke L22 to improve the voltage waveform (Fig. 3.7). However, the high-voltage bridge configuration (Fig. 3.7) does not provide the required load voltage of 220V when the choke is connected in the DC bus, only reaching 106V with an acceptable distortion factor (VH) ≤ 10%. When choke L2 is connected in the AC bus (Fig. 3.8 and 4.0), it achieves the desired voltage of 220V.In the high-voltage and low-voltage inputs, the minimum value for inductance

L2 is 40-60mH when connected in the AC bus (Fig. 3.6, 3.8, and 4.0). The high-voltage configuration (Fig. 3.7 and 3.8) does not have inverse current spikes in AB, while the low-voltage configurations (Fig. 3.5, 3.6, 3.9, and 4.0) have reverse current spikes proportional to the forward current. In the low-voltage bridge configurations (Fig. 3.9), the inductance L1 in the DC bus is 20μH, which is 1000 times smaller than the inductance L2 = 30mH in the AC bus (Fig. 4.0). The low-voltage configurations (Fig. 3.5, 3.6, 3.9, and 4.0) use automotive batteries AB with a voltage of 12-14V, while the high-voltage configurations (Fig. 3.7 and 3.8) require a series connection of 18 batteries, each with a voltage of 12V. The high-voltage DC link (Fig. 3.7 and 3.8) requires careful insulation of terminals and electrical connections on the roof to reduce leakage currents, especially during the rainy season. In the low-voltage configurations (Fig. 3.5, 3.6, 3.9, and 4.0), the currents VT, TV, and VD are an order of magnitude higher (10 times) than in the high-voltage configurations (Fig. 3.7,3.8). The equivalent levels of commutation voltages on the transistors in configurations (Fig. 3.5 and 3.6) are in the range of 200-220V. The advantage of the low-voltage bridge configuration with a step-up transformer (Fig. 3.9 and 4.0) is the low maximum voltage across the transistors VT1 to VT4, which is 14V for any connection of chokes L1 and L2. In the high-voltage configuration, it is recommended to connect choke L2 = 60mH in the AC bus (Fig. 3.8), while in the low-voltage configuration (Fig. 3.9), it is connected in the DC bus - L1 = 9.5mH. The capacitance of capacitor C2 is calculated to compensate for the load's inductive current and should be around 80 to 90μF. In all six configurations, the capacitance C2 = 170 to 200μF is connected in parallel to the load, ensuring a voltage waveform Kg (VH) <10%. In the low-voltage configuration (Fig. 3.5), to limit the switching overvoltage on VT, two shunt capacitors C1 and C3 of 100μF each, two diodes (VD3 and VD4), and two resistors (R1 and R2) are used, connected between the collectors of VT and + AB. The load parameters include a nominal active resistance RH = 19.36Ω, load inductance LH = 0.046H, and the load resistance varies from the nominal value to the no-load condition.

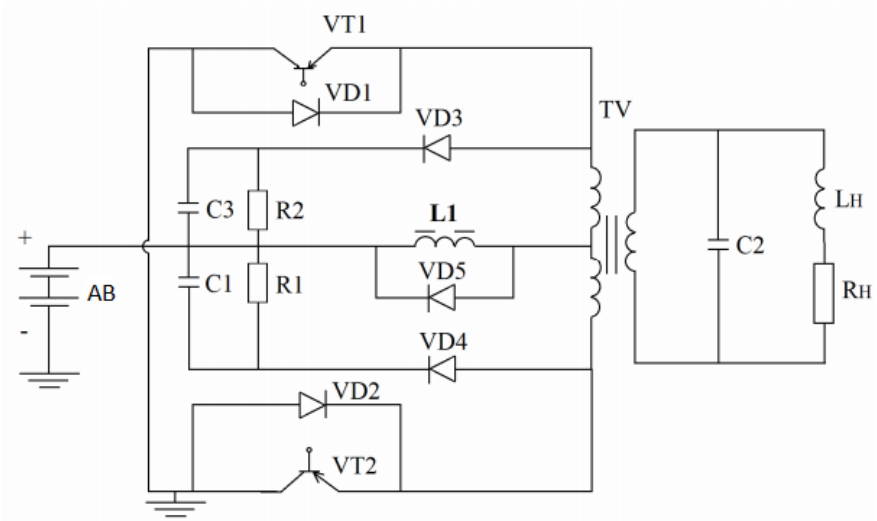

Figure 3.5- Low-voltage circuit with a direct current choke

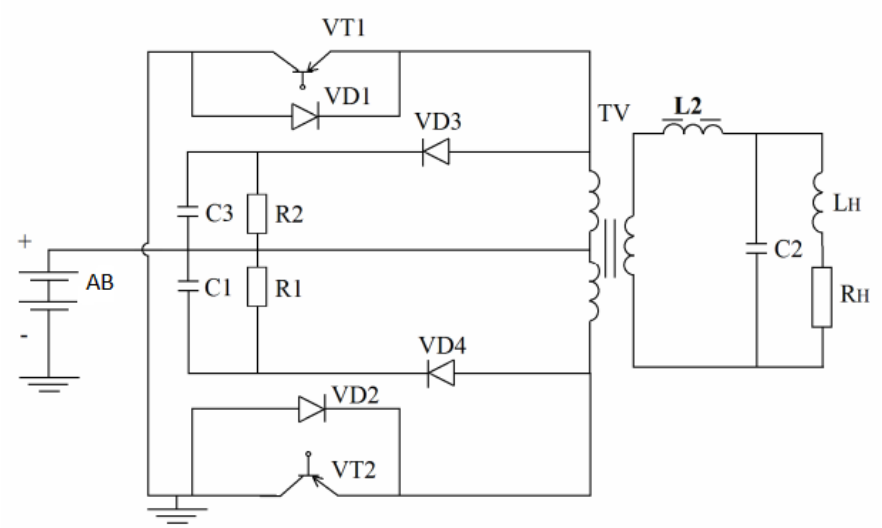

Figure 3.6- Low-voltage circuit with an alternating current choke

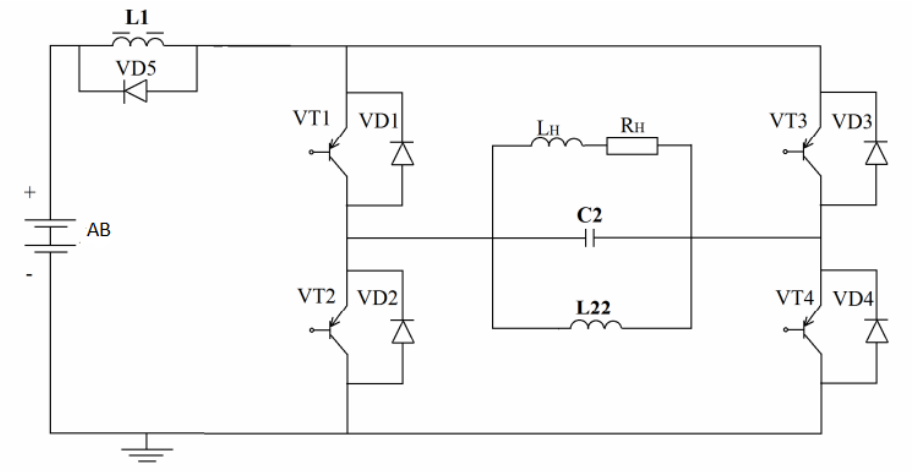

Figure 3.7- High-voltage bridge circuit with a direct current choke

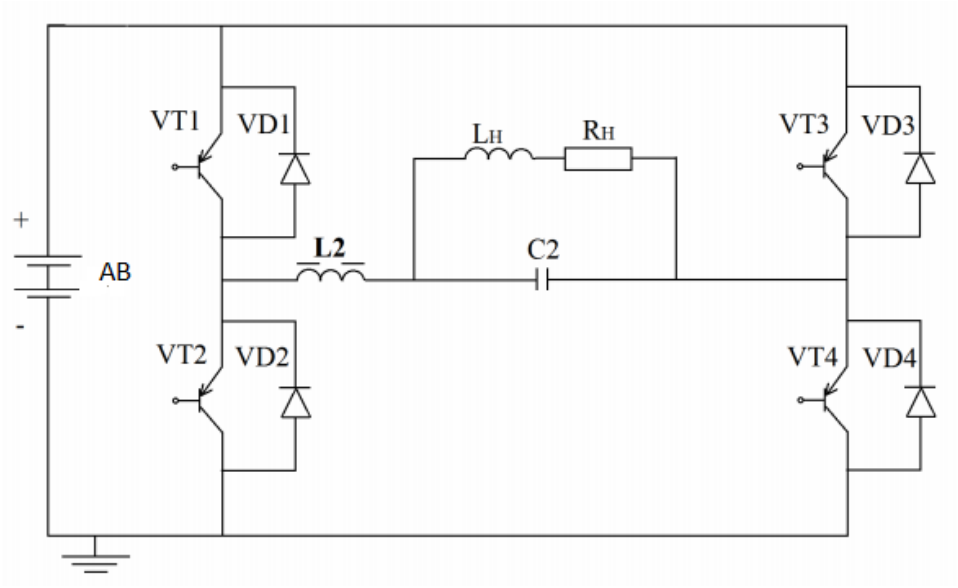

Figure 3.8- High-voltage bridge circuit with an alternating current choke

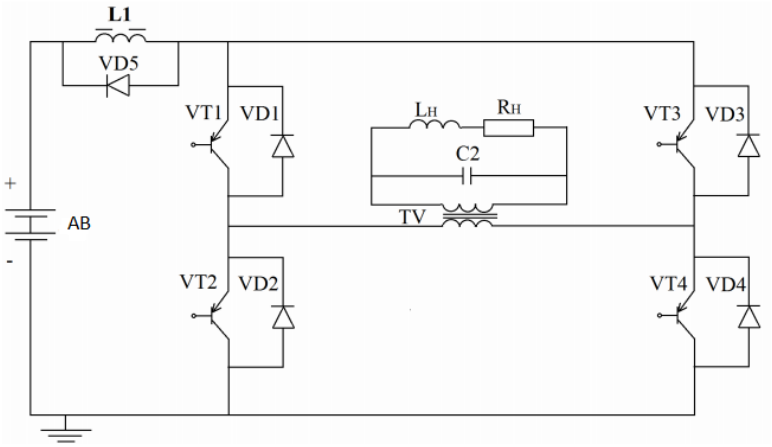

Figure 3.9- Low-voltage bridge circuit with a direct current choke

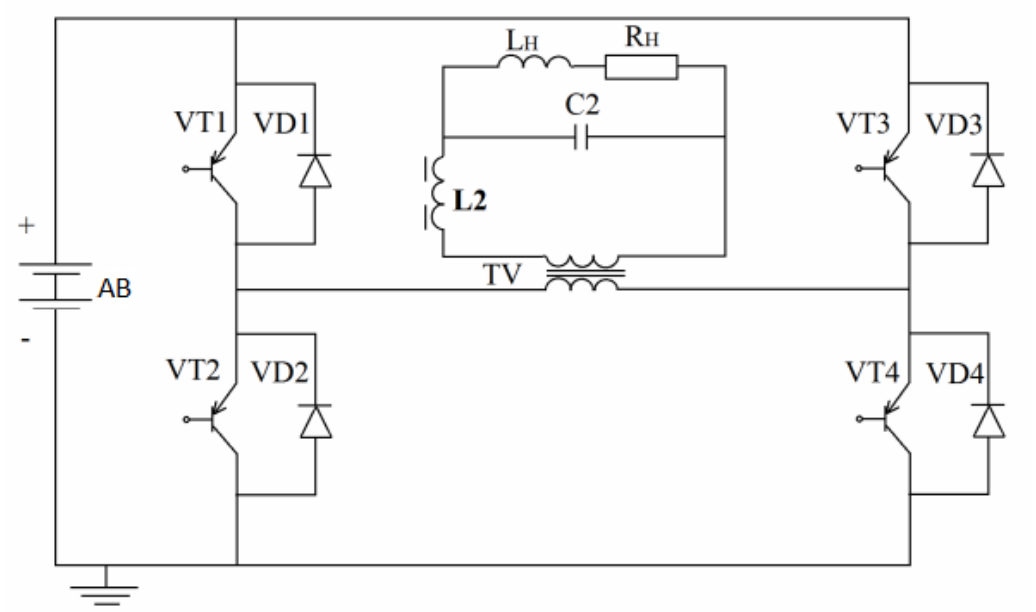

Figure 3.10- Low-voltage bridge circuit with an alternating current choke

Figure 3.11 shows the oscillograms of currents and voltages in the circuit (Figure 3.4), which demonstrate high quality of load current Kg (IH) = 2-4.4%, as well as

significant reverse current spikes from the power source up to Iobr = -350 A, with a forward current of Ipr = 274 A.

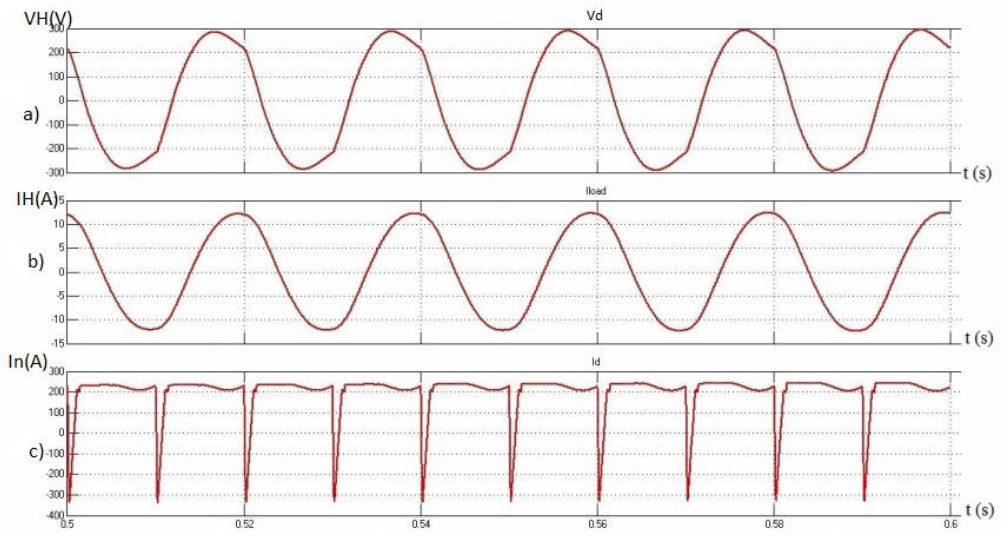

Figure 3.11- - Oscillograms of simulating the operating processes of the inverter: a) Voltage at the output of the inverter. b) Load current. c) Power source current.

The oscillograms of the power source current in the bridge circuit with an alternating current choke (Figure 3.10) are shown in Figure 3.12. It can be observed that the reverse current spike is small and equals Ip_{obr} = 5 A, while the forward current is Ip_{pr} = 13 A.

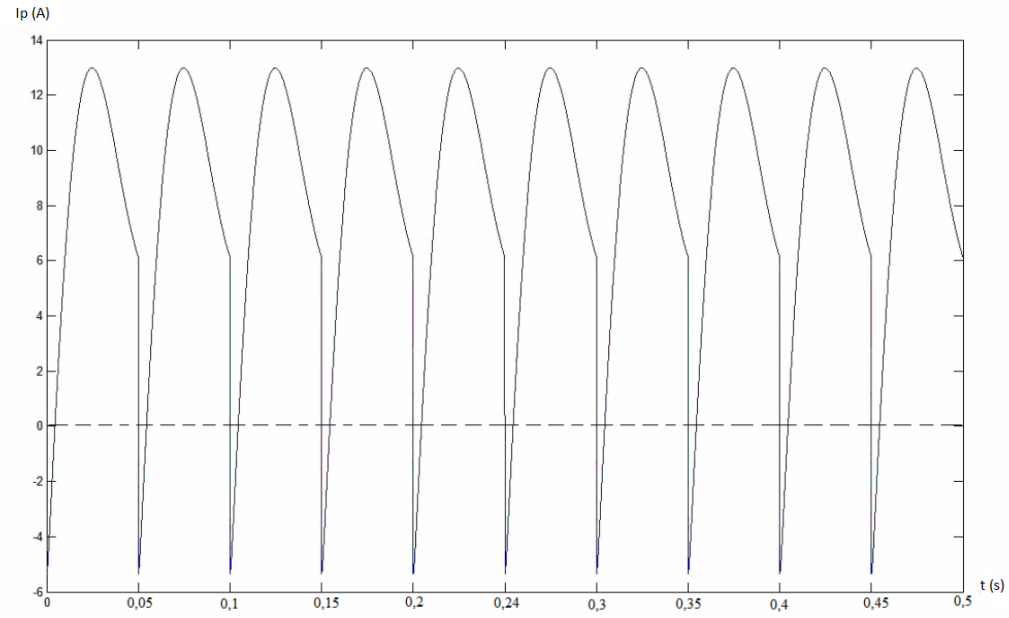

Figure 3.12- The oscillogram of current AB in a bridge circuit with an inductor for alternating current.

The selected modeling method in the MATLAB Simulink program allows for investigating all operating modes of the power electronics unit (PEU). For the high-

frequency inverter, the results of modeling and analysis of the asymmetric magnetization mode of the power transformer core in the two-pulse bridge circuits. In our case, the asymmetry coefficient is expected to be significantly lower due to the low-frequency inverter.

3.6 Study of the stability of the output voltage in a single-phase inverter according to the classical regulation algorithm (CRA)

The voltage at the input of the inverter changes U_{AB} = 10 ÷ 14, Ku = 1.4 – the ratio of the maximum value of the voltage to the minimum.

The aim of the study:

1. Stabilize the output voltage of the inverter to the value Ku = 1.1 (242/220), which meets the requirements of GOST, the voltage should vary from the nominal value by ± 10%.

2. Investigate an automatic adjustment algorithm that will ensure the minimum coefficient of harmonics of the output voltage at the lowest values of C - filter.

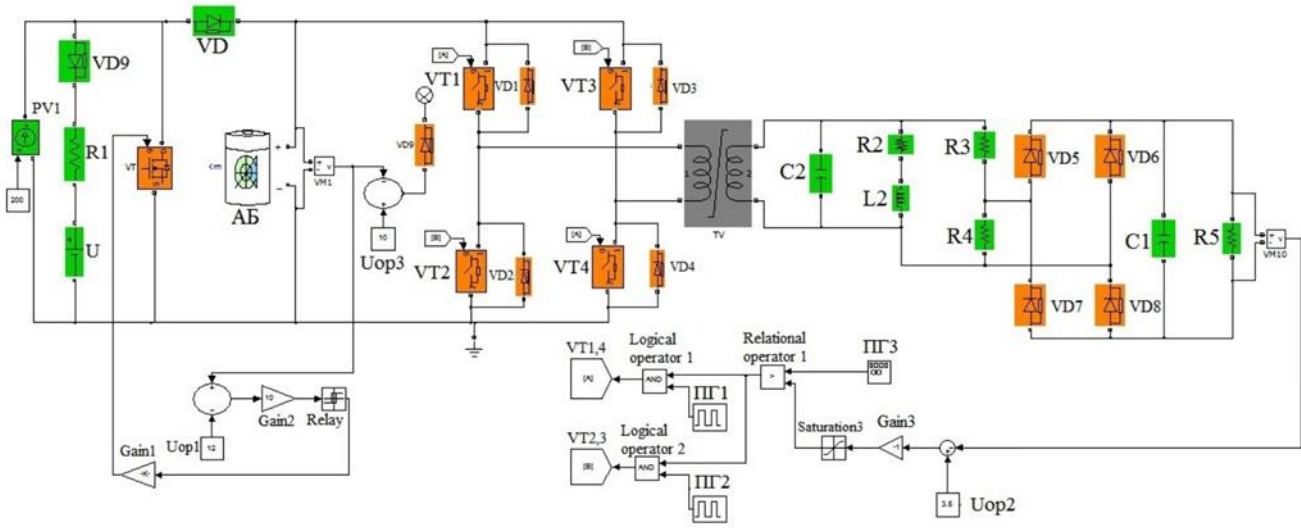

Figure 3.13 - Single-phase photoelectric power plant circuit for simulation in the Simulink program

The photoelectric power plant (Fig. 3.13) was modeled using the CRA of the output voltage (Fig. 3.14). The amplitude of the unfolding voltage is symmetrically triangular Up=2 V with a frequency f_P = 100 Hz and a reference voltage U_{OP} 2 = 3.5 V.

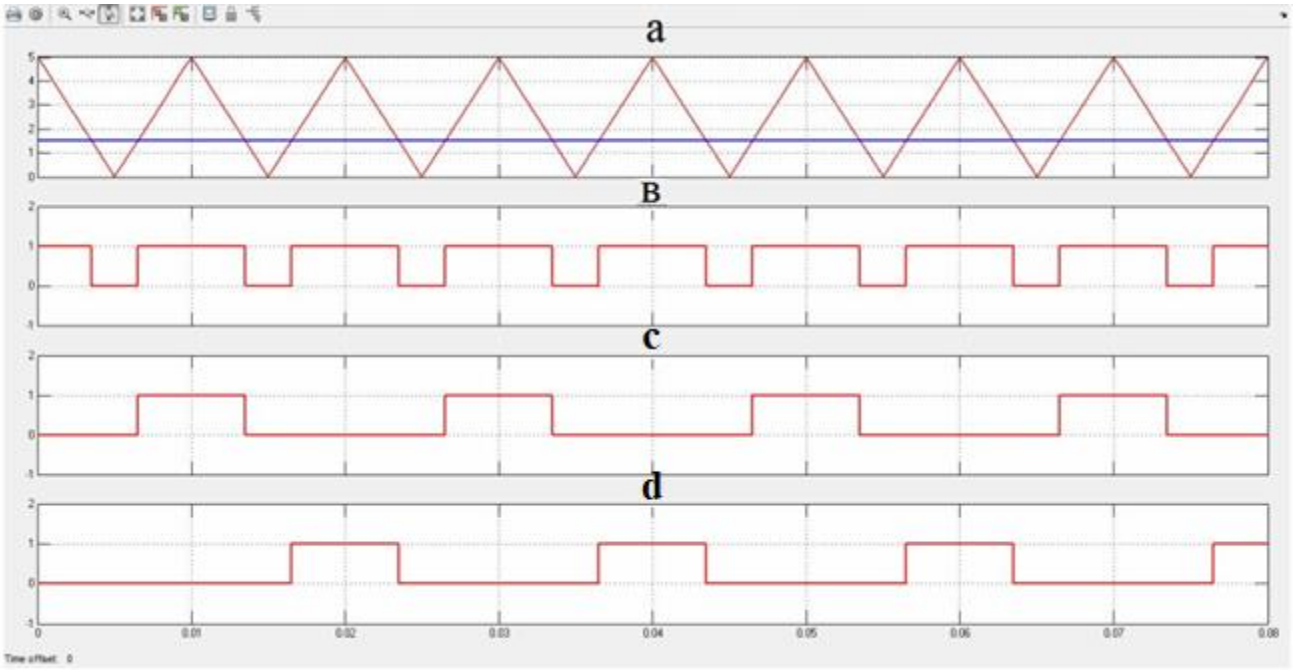

Figure 3.14 − Control algorithm for keys regulating U_L, a) comparison of the reference voltage with a sawtooth, b) signals after comparing Uop and Up, c) signals arriving at VT 1,4, d) signals arriving at VT 2 ,3.

The results of the simulation of the photoelectric power plant using the CRA of the output voltage at the input voltage U_{AB} = 14 V are shown in Fig. 3.15.

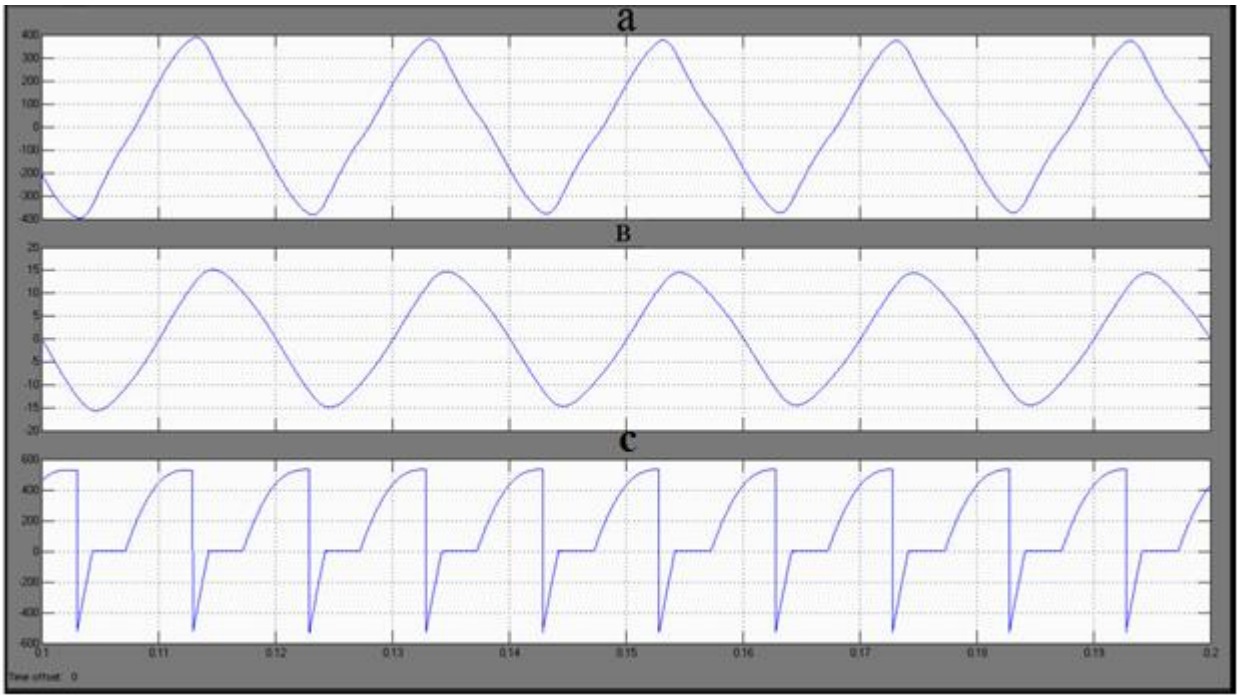

Figure 3.15 - Results of the simulation of the PV module: a) the output voltage of the inverter, b) the current flowing through the load, c) the current of the power source (at the input of the inverter)

The study showed that the CRA of the output voltage in fig. 3.13 ensures the required accuracy of the voltage level U_L = 220 V (± 10%) with an acceptable harmonic coefficient $K_h \leq 10\%$. Since inverters with a low harmonic ratio are mainly offered on the market, although $K_h \leq 10\%$ is enough for household consumption.

3.7. Relay Voltage Regulator

The relay voltage regulator is used to maintain a constant output voltage by adjusting the pulse duration of the transistors in the bridge circuit (Figure 3.16) when the input voltage V_{AB} varies from 10 to 14 volts. To perform this function, the inverter voltage V_L is reduced from 220 V to 7 V using a voltage divider consisting of resistors R3 and R4. The reduced voltage is rectified by diodes VD5 - VD8 and compared to a constant reference voltage Vop = 7 V in the "Relay Regulator" block. The outputs of this block, VT 2,3 and VT 1,4, control the power transistors VT1 - VT4 and ensure a nominal voltage VL = 220 V. The outputs VT 2,3 and VT 1,4 of the "Relay Regulator" block are connected to the control inputs VT 2, VT3 and VT1, VT4, respectively. When the rectified voltage VR5 exceeds the reference value of 7 V, the transistors VT1 - VT4 are turned off, and when it drops below 7 V, they have turned on again (Figure 3.17). The simulation results are presented in Table 5, and the oscillograms are shown for V_{AB} = 10 V in Figure 3.18 and for V_{AB} = 14 V in Figure 3.19.

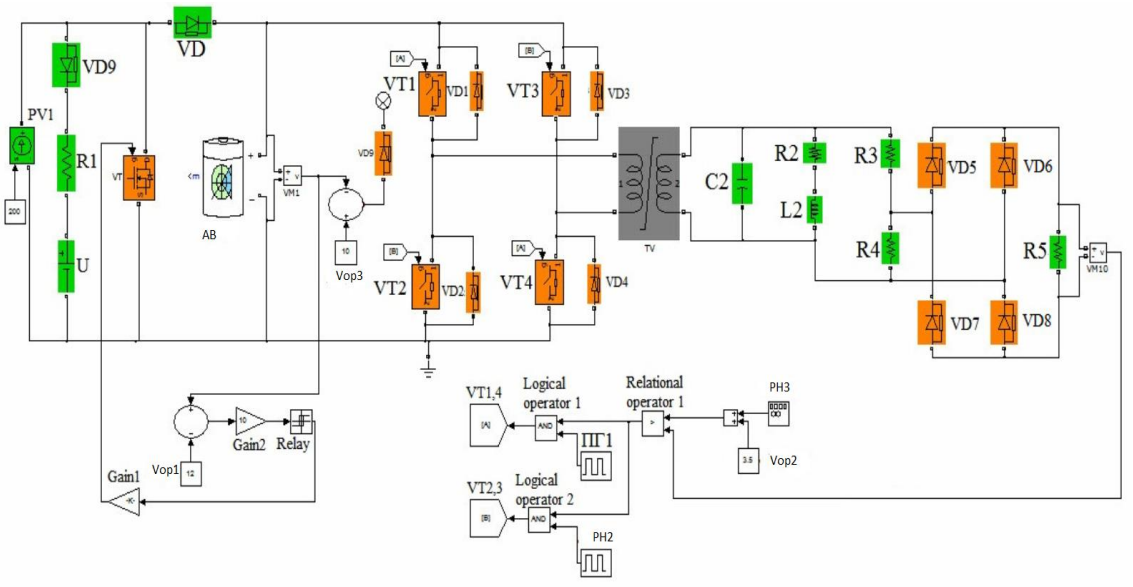

Figure 3.16 - A single-phase inverter with output voltage stabilization implemented in Simulink.

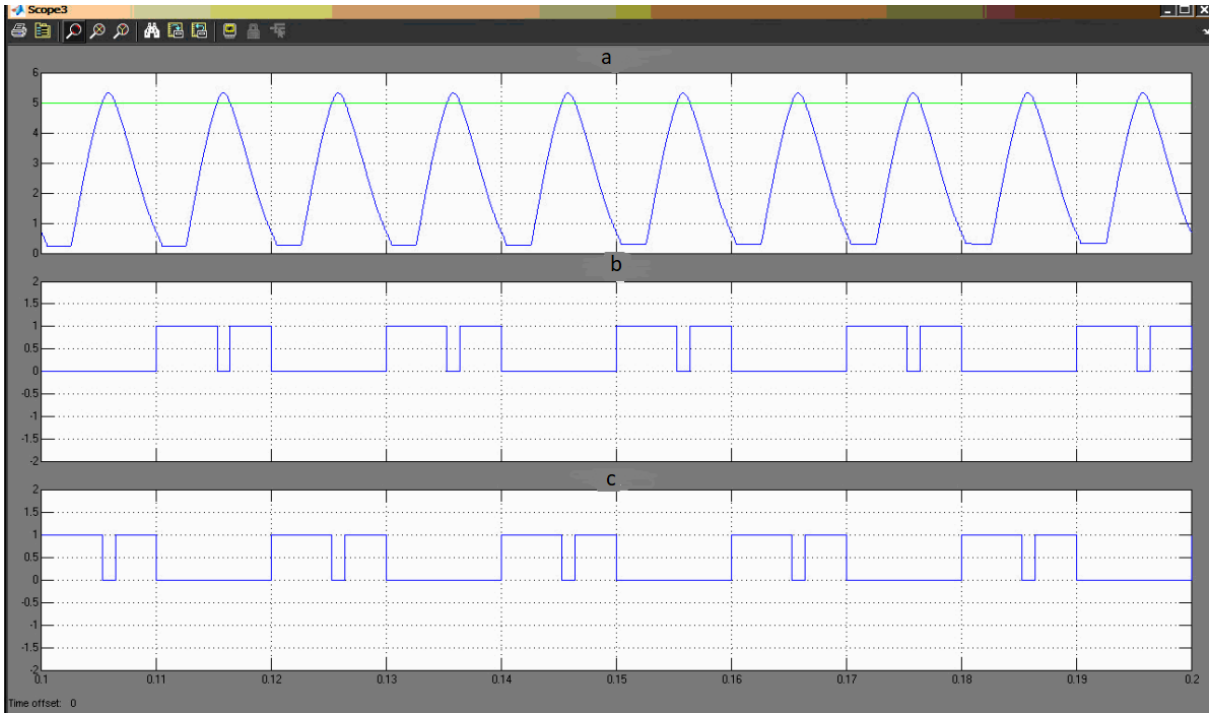

Figure 3.17 - a) Comparison of rectified voltage with the reference voltage: This plot shows the comparison between the rectified voltage (VR5) and the reference voltage (Vop). It indicates how the rectified voltage is compared to the reference voltage to determine the control actions of the system.

b) Pulses for transistors VT1 and VT4: This plot displays the pulse signals generated for transistors VT1 and VT4. These pulses control the switching behavior of the transistors in the inverter circuit.

c) Pulses for transistors VT2 and VT3: This plot illustrates the pulse signals generated for transistors VT2 and VT3. These pulses control the switching behavior of the transistors in the inverter circuit.

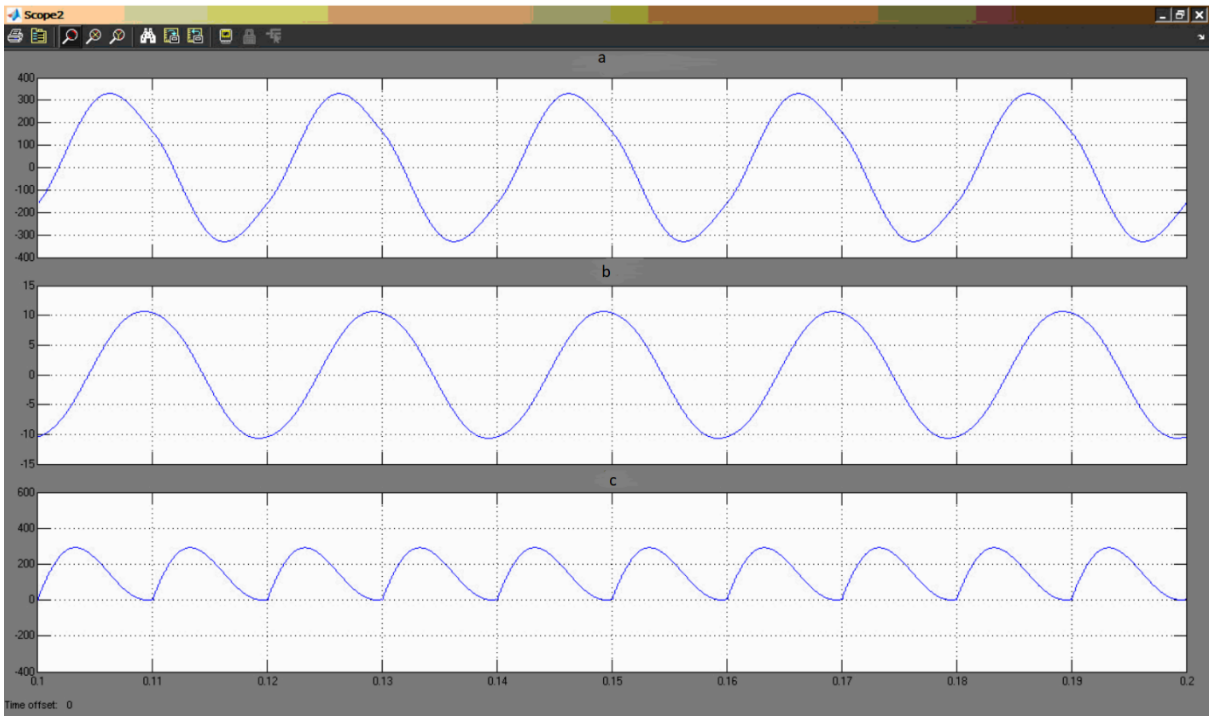

Figure 3.18- Simulation oscillograms at V_{AB} = 10 V:

a) Voltage at the inverter output

b) Load current

c) Power supply current

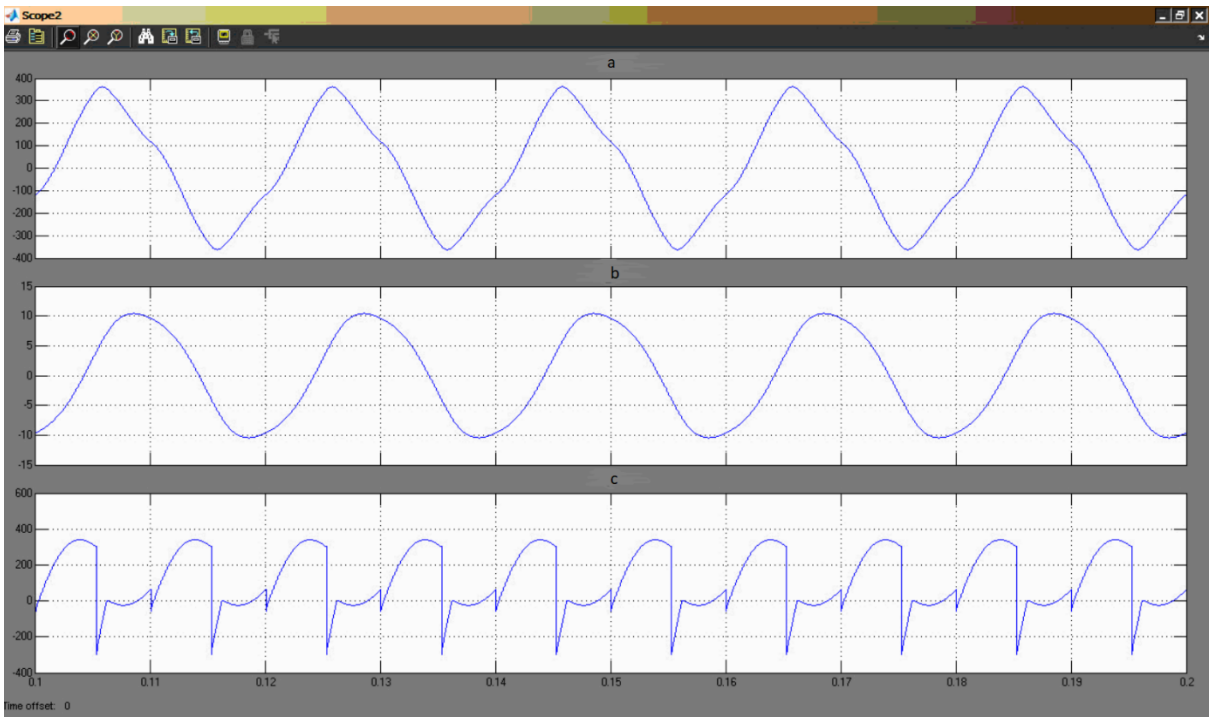

Figure 3.19 - Simulation oscillograms at V_{AB} = 14 V:

a) Voltage at the inverter output

b) Load current

c) Power supply current

Table 3.2 shows the dependence of the load voltage V_L and the coefficient of nonlinear distortions K_h on the voltage V_{AB}.

Table 3.2 Simulation Results

AB voltage, V_{AB} (V)	Load voltage, V_{L1} (V)	The coefficient of nonlinear distortion K_h (V_{L1}) (%)
10	221.1	5.71
11	231.6	6.68
12	230.7	13.47
13	228	12,28
14	225.1	13.65

When the AB voltage is varied from 10 to 14 volts using relay regulation, the output voltage of the inverter is maintained within the range of V_{L1}= 221.1 to 231.6V. The harmonic distortion coefficient in this case is $K_h(V_{L1})$ = 5.71 to 14%. Overall, this regulation method operates quickly and the circuit is simple. Its use for domestic consumption is completely permissible.

3.8 Pulse Width Modulation (PWM) controller

In the voltage regulation based on Pulse Width Modulation (PWM) (Fig. 3.20), a sawtooth reference voltage is compared with the rectified mains voltage reduced by a voltage divider to the value of the reference sawtooth voltage. The amplitude of the sawtooth voltage is 10V when VAB is in the range of 10V to 14V. The pulses of the sawtooth voltage open the power transistors when the rectified mains voltage exceeds the sawtooth voltage, and the transistors close when the rectified mains voltage falls below the sawtooth voltage (Fig. 3.20). The inverter circuit corresponds to Fig. 3.16, where the Relay Regulator module contains a pulse generator for the reference voltage with an amplitude of 10V and a frequency of 1000 Hz. The simulation results are shown in Fig. 3.21.

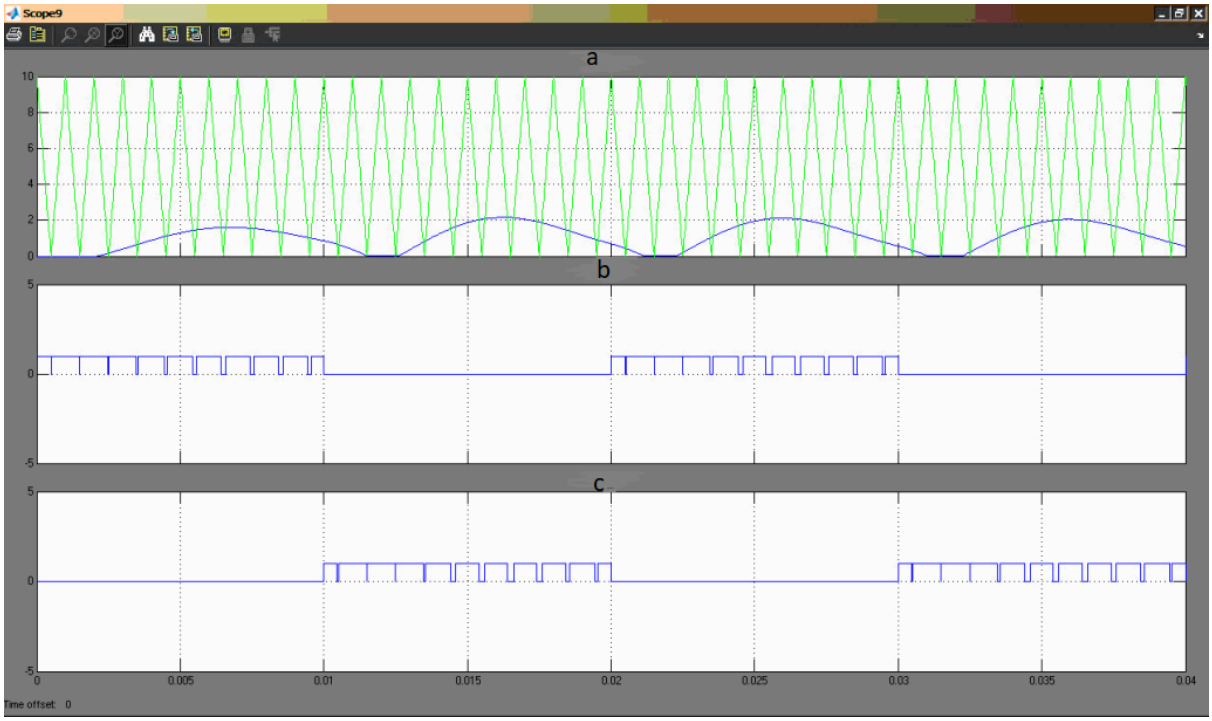

Figure 3.20- a) Comparison of rectified voltage with reference voltage.
- b) Pulses for transistors VT1 and VT4.
- c) Pulses for transistors VT2 and VT3.

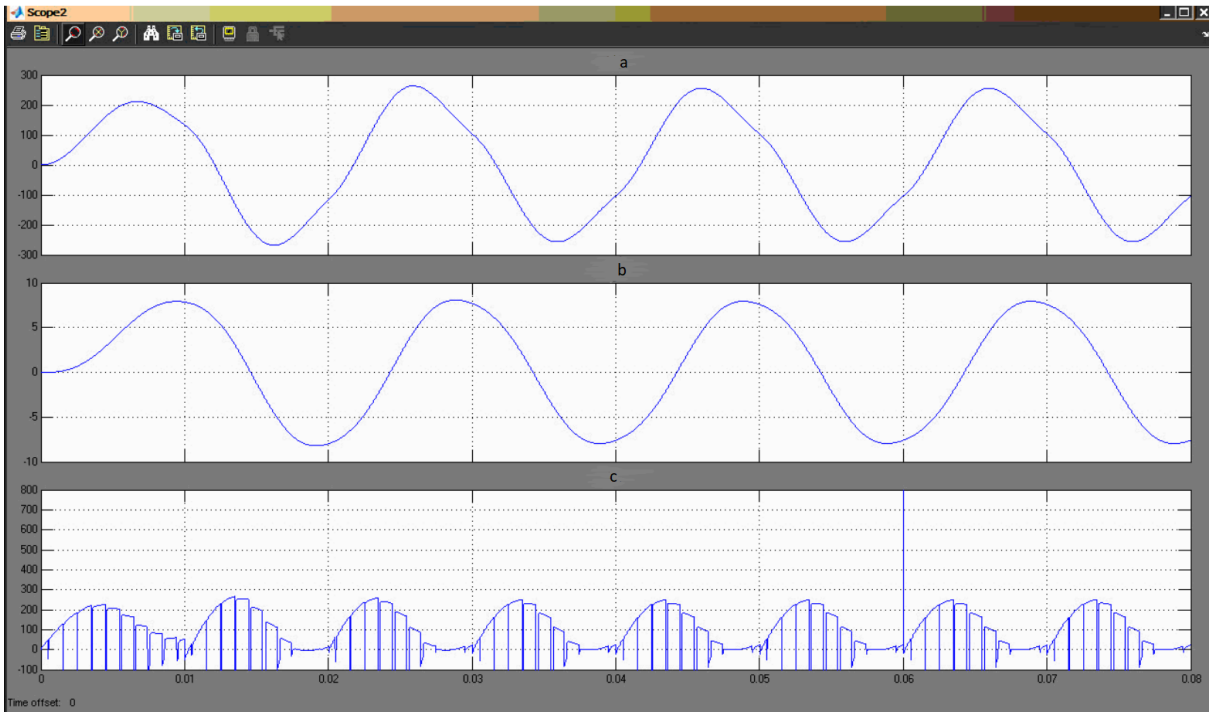

Figure 3.21. Simulation oscillograms at VAB = 14 V:
a) Voltage at the output of the inverter.
b) Load current.
c) Power supply current.

Table 3.3 provides the dependencies of the load voltage V_L and the coefficient of nonlinear distortions K_h on the input voltage AB - V_{AB}.

Table 3.3. Simulation Results

AB voltage, V_{AB} (V)	Load voltage, V_{L1} (V)	the coefficient of nonlinear distortions K_h (V_{L1}) (%)
10	221.1	5.71
11	231.6	6.68
12	230.7	13.47
13	228	12.28
14	225.1	13.65

In this circuit, parametric voltage stabilization is implemented, but sinusoidal PWM generation is absent. From the perspective of voltage waveform, the reverse logic has emerged, where the pulse duration at the edges of the half-cycle increases. Additionally, the stability of the output voltage is low. The investigation revealed that when the AB voltage changes by 40% - from 10 to 14 volts - the output voltage varies by 25% - from 221.3 V to 277.1 V. This method does not provide the necessary voltage range change of ±10% since it achieves a range of ±25%. However, a positive characteristic of this regulation method is the low and minimally variable distortion coefficient K_h (V_{L2}) = 4.03 to 4.82%.

3.9 Conclusions on the section:

1. The calculated area of the solar module (SB) based on the average load power and specific power of the SB is SCB = 7.05 m^2. For the design of the photovoltaic power generation system, an SB with an efficiency of 15% and an area of S_{SB} = 12 m^2 is used.

2. For the selection of the battery capacity (AB), the energy balance calculation method was utilized. The option with the highest nominal capacity of Q_{AB} = 1000 Ah (ampere-hours) or N_{AB} = 5 units was chosen.

3. Six different photovoltaic power generation system configurations were investigated, varying in SB voltage, AB configuration, and the inclusion of a smoothing inductor on the AC bus and DC bus. This study allowed the selection of the optimal

configuration: a low-voltage configuration with a single-phase voltage inverter using a bridge circuit. This configuration eliminates overvoltage on the transistors and reverse current in the AB.

4. The influence of load variation on the system operation was examined and showed that the harmonic distortion coefficient for a power factor of 0.8 varied from 3.15% to 10.15% under nominal load and varying AB voltage. For an active load, the distortion coefficient K_h (V_L) ranged from 4.46% to 5.71% from nominal load to no-load condition. The developed inverter can be used for various household electrical appliances.

5. Two methods of automatic voltage stabilization for the inverter were considered: relay voltage regulator and pulse-width modulation (PWM) regulator. The relay regulator maintains the voltage within the range of V_{L1} = 221.1 to 231.6 V, with a harmonic distortion coefficient K_h (V_{L1}) ranging from 5.71% to 14%. The PWM regulator maintains V_{L2} = 221.3 to 277.1 V, with a distortion coefficient K_h (V_{L2}) ranging from 4.03% to 4.82%.

4 SAFETY OF LIVELIHOOD AND FUNDAMENTALS OF LABOR PROTECTION

4.1 **Ultraviolet Radiation and Its Effects On The Body**

Ultraviolet (UV) radiation is characterized by a dual action, as its influence can be both positive and negative. The biological effects of UV radiation from sunlight primarily manifest in its positive impact on the human body. UV exposure is an essential factor for life. Prolonged lack of sunlight can disrupt the physiological balance of the body, leading to a complex of symptoms known as "light starvation." The most common consequences of insufficient sunlight exposure include weakened immune responses, exacerbation of chronic conditions, and functional disorders of the nervous system. This particularly affects workers in mines or poorly lit and windowless facilities, where natural lighting is absent. Mild doses of UV radiation have a beneficial effect on the body, normalizing blood pressure, metabolic processes, increasing resistance to illnesses, improving cold tolerance, and reducing fatigue.

UV radiation from occupational sources can cause acute and chronic professional diseases. The visual system is particularly susceptible to the effects of UV radiation. Acute eye damage due to UV exposure is called electro-ophthalmia (or photokeratitis). It is characterized by sensations of foreign objects or sand in the eyes, light sensitivity, and excessive tearing. Chronic professional diseases associated with UV radiation include conjunctivitis and cataracts. Skin diseases can manifest as acute dermatitis with erythema and sometimes oedema, leading to blister formation. In addition to local reactions, general toxic effects may occur, such as increased body temperature, fever, headaches, and digestive disturbances. Sunburn is the classic skin damage caused by UV radiation. Chronic changes in the skin due to UV exposure manifest as "photoaging" (solar elastosis), epidermal atrophy, and the potential development of malignant neoplasms. In industrial settings, the most significant concern is professional

sensitization to ultraviolet radiation within the solar spectrum, leading to severe forms of keratoconjunctivitis, dermatitis, and general toxic effects.

To prevent "UV deficiency," various measures are employed, including sunlight exposure through room insolation, light and air baths, tanning beds, and artificial UV sources. Preventive measures to address "UV insufficiency" are regulated by sanitary legislation. Work premises where employees spend extended periods and lack natural lighting or where biological effects of light are insufficient according to sanitary norms are equipped with UV radiation devices (with erythemal lamps). Preventive measures for preventing electro-ophthalmia involve using protective eyewear or face shields during tasks such as electric welding and others. Protective clothing, sunscreens, and creams are used to shield the skin from UV radiation. Permissible levels of UV exposure and irradiation vary depending on the UV source, and there are regulations for the total duration of work. Protective measures include materials that reflect UV radiation and protective screens for the skin and eyes. Protective clothing should have long sleeves and a hood. Eyes are safeguarded using light-protective goggles (with nitro-filters) with regular lenses or lenses containing lead oxide. In order to prevent it, rational organization of work and rest schedules, appropriate placement of workstations, and keeping them at a distance from powerful UV sources are utilized.

4.2 Electrical Safety and Types of Electrical Injuries

Modern production is closely associated with the use of electrical energy. In the conditions of operating powerful energy systems, electrical machinery and devices, development of computer technology and instrumentation, automation, and computerization of production, the issue of electrical safety becomes crucial. It involves protecting electrical personnel and other individuals who handle electrical equipment from electric shock. An analysis of the overall number of occupational accidents indicates that the percentage of electrical injuries ranges from 1.0-1.5%, and in the energy sector, it can reach 3-5%. However, among fatal accidents, electrical injuries account for 20-40% in general production and up to 60% in the energy sector, occupying a prominent position. Electrical injuries occur when a person comes into

contact with elements of electrical installations with different potentials or potentials that differ from the ground potential, resulting in the formation of an electric arc either between the elements of the electrical installation directly or between the elements and a person in contact with the ground. They can also occur due to the effects of step voltage.

Electrical trauma, as a social category, is characterized by the total number of electrical injuries within a certain period of time, their absolute and relative indicators, distribution by severity, and industrial sectors. In general, industrial trauma, electrical injuries account for about 1%, while in fatal cases, they comprise about 15-20%. This indicates a shift towards more severe types of electrical injuries, which is one of the peculiarities of electrical trauma. Another peculiarity is that electrical injuries with fatal consequences constitute up to 70-80% for electrical installations with a voltage of up to 1 kV and 20-30% for electrical installations with a voltage above 1 kV. Compared to other types of injuries, electrical trauma has the following characteristics:

- A person is unable to remotely determine the presence of voltage without special devices, so the effect of the current is usually sudden, and the body's protective reaction manifests only after coming into contact with the current.

- The current flowing through the human body affects tissues and organs not only at the points of contact with the current-carrying parts and along the current path but also reflexively, as an extremely strong stimulus, influencing the entire organism. This can lead to disruptions in the functioning of vital systems such as the nervous, cardiovascular, and respiratory systems.

- Electrical injuries can occur without direct contact between a person and the current-carrying parts due to the formation of an electric arc between the current-carrying parts or between the current-carrying parts and the person or ground.

- Investigation, recording, and analysis primarily focus on severe electrical injuries and those resulting in fatalities, which negatively affects the prevention of electrical injuries.

The flow of current through the human body is accompanied by thermal, electrolytic, and biological effects. The thermal effect of the current involves tissue heating, evaporation of moisture, which causes burns, charring of tissues, and steam

ruptures. The severity of the thermal effect of the current depends on the magnitude of the current, the resistance to the current flow, and the duration of the current flow. In cases of short-duration current flow, the thermal component can be decisive in the nature and severity of the injury. The electrolytic effect of the current manifests in the decomposition of organic substances (electrolysis), including blood, leading to changes in their physicochemical and biochemical properties. This, in turn, disrupts the biochemical processes in tissues and organs, which are essential for the organism's vital functions. The biological effect of electric current manifests itself in the irritation and disturbance of living tissues in the body, including at the cellular level. This disrupts the internal bioelectrical processes that occur in a normally functioning organism and are related to its vital functions.

Ensuring the safe operation of solar power installations. The head of the enterprise is obliged to ensure the maintenance, operation, and servicing of solar power installations in accordance with the requirements of applicable regulatory documents. To do this, he must:

- Appoint a person responsible for the proper condition and safe operation of the electrical system from among the engineering and technical personnel who have received electrical training and passed the knowledge assessment in the established procedure (the person responsible for the electrical system).

- Ensure an adequate number of electrical personnel.

- Approve the regulations on the energy service of the enterprise, as well as job descriptions and instructions for labor protection.

- Establish procedures to ensure that employees entrusted with the maintenance of solar power installations carefully monitor the assigned equipment and networks, conducting inspections, performance checks, tests, and measurements.

- Ensure the implementation of emergency, acceptance-testing, and preventive tests and measurements of electrical installations in accordance with the rules and norms (Electrical Safety Rules).

- Ensure the conduct of technical inspections of solar power installations.

4.3 Characteristics of the Negative Impact and Protective Measures Against Natural Disasters That Can Disrupt the Operation of Energy Facilities.

Natural disasters are phenomena that create a catastrophic situation, disrupt normal population activities, destroy buildings and structures, threaten lives, and lead to the loss of human and animal lives and destruction of material values. Natural disasters are very dangerous because of their sudden occurrence. They cause significant damage to energy facilities.

There are types of natural disasters such as mass forest fires, earthquakes, floods, catastrophic floods, snowdrifts, landslides, avalanches, and hurricanes. Natural disasters or industrial accidents that result in loss of life are called catastrophes. The following types of natural disasters are distinguished: meteorological disasters - storms, hurricanes, typhoons, cyclones, extreme cold, and droughts; topological disasters - floods, landslides, and snowslides. They usually occur due to excessive precipitation, intense snow and ice melting, and ice jams. Tectonic disasters include earthquakes, tsunamis, and volcanoes. Earthquakes are one of the most terrifying types of natural disasters, accompanied by human casualties and the destruction of energy facilities. According to UNESCO, earthquakes are the first in terms of damage and of the first in terms of the number of people killed. In European countries, the 12-point international MSK-64 scale is used to determine the intensity of earthquakes. The first category includes earthquakes, hurricanes, floods, fires, and epidemics that affect a territory exceeding the administrative boundaries of the region and those that cause significant material damage to the economy.

To eliminate the consequences of natural disasters, it is necessary to use the units of the Operational Rescue Service of Civil Protection, civil defence formations and specialized departmental formations. The second category includes natural disasters whose effects affect the territory within the administrative boundaries of the region and cause material damage to the national economy. To eliminate the consequences of such disasters, local authorities, executive authorities, and relevant organizations must mobilize their forces and means in a timely and efficient manner.

Natural disasters are catastrophic events caused by natural phenomena that disrupt normal human activities, destroy buildings and structures, endanger lives, and result in the loss of human and animal lives as well as the destruction of material assets. Natural disasters are particularly dangerous due to their sudden occurrence and can cause significant damage to energy facilities.

There are various types of natural disasters, such as large-scale forest fires, earthquakes, floods, catastrophic flooding, snowdrifts, mudflows, avalanches, and hurricanes. Natural disasters or industrial accidents resulting in human casualties are referred to as disasters. The following types of natural disasters are distinguished: meteorological disasters (storms, hurricanes, typhoons, cyclones, extreme cold, droughts), topological disasters (floods, mudflows, avalanches, snowslides), and tectonic disasters (earthquakes, tsunamis, volcanoes). Earthquakes are one of the most terrifying types of natural disasters, causing human casualties and destruction of energy facilities. According to UNESCO, earthquakes rank first in terms of damage and are among the leading causes of human fatalities. In European countries, the 12-point MSK-64 international scale is used to determine the intensity of earthquakes. Protection of the population and industrial personnel from the consequences of natural disasters, major accidents, and catastrophes is ensured by the Civil Protection Code which includes sheltering in protective structures, the use of personal protective equipment, and evacuation from hazardous areas. Sheltering is provided in existing protective shelters and anti-radiation shelters. It is important not only to construct protective structures but also to maintain them in a state of constant readiness. Measures have been developed by civil protection authorities in collaboration with the heads of ministries, departments, national economy facilities, regions, cities, and districts to provide population residing in hazardous zones with protective structures and personal protective equipment. Timely notification of the population about the threat of natural disasters, accidents, and catastrophes is one of the essential measures of civil protection. Centralized warning systems in the areas of nuclear power plants and hazardous chemical facilities are kept in constant readiness. Measures are taken to ensure that the notification process for the leadership and local civil protection authorities is simple and reliable, including remote activation of sirens, radio broadcast points, and other

technical warning devices. Hurricanes and tornadoes are extremely fast and powerful air movements that often result in human casualties, destruction of marine and river vessels, damage to buildings, structures, and energy facilities, and sometimes entire settlements. Tornadoes are vortices that can exceed the speed of sound. The air pressure drop within a tornado is so significant that it can uproot trees, tear off roofs, topple wooden houses, and completely destroy them. In such cases, the safest places to seek refuge are basements, ditches, trenches, warehouses and civil defence shelters.

GENERAL CONCLUSIONS

In the presented qualification work, the following conclusions can be drawn:

1. To construct the Photovoltaic Energy Facility model, a solar cell model called the "single diode model" was proposed. The influence of the diode ideality factor and the reverse saturation current on Vxx (voltage across the load) was simulated. It was shown that as the diode saturation current increases from I0=400 μA to I0=4000 μA, Vxx decreases from 21.6 to 19 V, resulting in a decrease in output power.

2. The PV structure with the simplest protection and control circuitry between the solar battery (SB) and the load battery (AB) was chosen. The solar panels were installed on the roof with a tilt angle of $\beta = 40°$, providing 1906 kWh/m^2 per year. By installing SB on rooftops, the use of solar energy becomes feasible in remote areas.

3. The area of the solar battery (SB) was calculated based on the equality of the average load power and the average specific power of SB - $S_{SB} = 7.05$ m^2. For the design, SB with an efficiency of 15% and an area of $S_{SB} = 12$ m^2 is used.

4. The selection of the battery capacity (AB) was based on energy balance calculations. The option with the highest nominal capacity of $Q_{AB} = 1000$ Ah ($N_{AB} = 5$ units) was chosen.

5. The influence of load variation on the design operation was investigated. It was found that the harmonic distortion coefficient at $\cos \varphi = 0.8$ ranges from 3.15% to 10.15% at nominal load and varying AB voltage. For active load, the coefficient K_h (V_L) varies from 4.46% to 5.71% from nominal to idle state. The developed system can be used for any household electrical appliances.

6. Two methods of automatic output voltage stabilization of the converter were considered: a relay voltage regulator and a pulse width modulation (PWM) regulator. The relay voltage regulator maintains the voltage within the range of $V_{L1} = 221.1$ to 231.6 V, with a harmonic distortion coefficient of K_h (V_{L1}) = 5.71% to 14%. The PWM regulator maintains $V_{L2} = 221.3$ to 277.1 V, with a distortion coefficient of K_h (V_{L2}) = 4.03% to 4.82%.

REFERENCES

1. Andreev V.M.: Optimization of Parameters of Solar Modules Based on Lens Concentrators of Radiation and Cascade Photovoltaic Converters, Journal of Technical Physics - 2010, Vol. 80, Issue 2 - 259 pages.
2. Andreev V.M.: Photovoltaic Conversion of Concentrated Sunlight, Leningrad: Nauka, 1989 - 310 pages.
3. Batluk V.A.: Occupational Safety in the Telecommunications Industry: a Training Manual, Lviv: Afisha, 2003 - 320 pages.
4. Zvereva, S.V.: In the World of Solar Light: Gidrometeoizdat, 1988 - 121 pages.
5. Kitaeva M.V., Yurchenko A.V., Okhorzina A.V., Skorokhodov A.V.: Autonomous Sun Tracking System for Solar Energy Systems: Polytechnic Herald, 2011 - No. 3/1 - 365 pages.
6. Kosenko V.F., Simenenko S.T.: Energy Conservation: a Training Manual, Luhansk: Vyd-vo SNU im.V.Dalya, 2012 - 214 pages.
7. Malyarenko V.A., Lisak L.V.: Energy and Environmental Energy Saving, Kharkiv: "Rubikon," 2004 - 215 pages.
8. Moskalova M.V., Batlukh V.A., Kuskovets S.L., Filipchuk V.L.: Occupational Safety (Questions and Answers): a Training Manual, Kyiv: Nauka, 2012 - 468 pages.
9. Pedan M.P., Rogozhin P.S., Skursky M.A.: Management of Production Economics, Kyiv: Vysha shkola, 1990 - 294 pages.
10. Sagitov P.I., Tsyba Yu.A., Daraev A.M.: Influence of Mechanical Vibrations on the Power of the SFES Electric Drive: Herald of PSU, 2008 - No. 4 - 224 pages.
11. Steblyuk M.I.: Civil Defence and Civil Protection: a Textbook, Kyiv: Znannia, 2006 - 487 pages.
12. Torkatiuk V.I., Momot T.V., Nokhrina L.A.: Guidelines for the Organization of Diploma Design (Writing Master's Theses) and Implementation of Diploma Projects (Master's Theses)
13. Legue, A.: Handbook of Photovoltaic Science and Engineering , A. Be-gue,

S. Hegedus – John Wille & Sons, Ltd, 2003 – 255 p.

14. Placko D. Fundamentals of Instrumentation and Measurement / D. Placko, ed. – London: ISTE Ltd. - 2007. - 532 p.

15. Scott J. Pulsed device measurements and applications / J. Scott, J. Rathmell, A. Parker, M. Sayed //IEEE Transactions on Microwave Theory and Techniques. Vol. 44. – 1996. – No. 12. - P. 2718 - 2723.